IOP Publishing Journal of Optics

J. Opt. **12** (2010) 093001 (20pp) doi:10.1088/2040-8978/12/9/093001

REVIEW ARTICLE

Spatio-temporal couplings in ultrashort laser pulses

Selcuk Akturk[1], **Xun Gu**[2], **Pamela Bowlan**[3] **and Rick Trebino**[3]

[1] Department of Physics, Istanbul Technical University, Maslak 34469, Istanbul, Turkey
[2] Max-Planck-Institute of Quantum Optics, Hans-Kopfermann-Straße 1, D-85748 Garching, Germany
[3] Georgia Institute of Technology, School of Physics, 837 State St NW, Atlanta, GA 30332, USA

Received 1 June 2010, accepted for publication 20 July 2010
Published 27 August 2010
Online at stacks.iop.org/JOpt/12/093001

Abstract
The electric field of an ultrashort laser pulse often fails to separate into a product of purely temporal and purely spatial factors. These so-called spatio-temporal couplings constitute a broad range of physical effects, which often become important in applications. In this review, we compile some recent experimental and theoretical work on the understanding, avoidance and applications of these effects. We first present a discussion of the characteristics of pulses containing spatio-temporal couplings, including their sources, a mathematical description and the interdependence of different couplings. We then review different experimental methods for their characterization. Finally, we describe different applications of spatio-temporal couplings and suggest further schemes for their exploitation and avoidance.

Keywords: ultrafast optics, pulse measurement

(Some figures in this article are in colour only in the electronic version)

1. Introduction

Since the advent of ultrashort-pulsed lasers there has been an ever-increasing interest in them, from both the scientific and industrial communities. What makes these sources so appealing is mainly their ability to harness light in time by squeezing pulse durations down to femtoseconds. As a result, ultrashort laser pulses have became indispensable for investigating and controlling ultrafast phenomena—events happening on picosecond or femtosecond timescales—such as chemical reactions, plasma dynamics, magnetization dynamics and others [1–3]. Additionally they make it possible to achieve unprecedented intensity levels in an electric light field, accessing a myriad of light–matter interactions [4, 5].

Ultrashort pulses are commonly described by the temporal variation of their power density and frequency, i.e. their intensity and phase. The dependence of the pulse's electric field on spatial coordinates is often treated separately, assuming that the pulse's temporal properties are the same for every spatial position along the beam, or equivalently, that the pulse's field separates into a product of temporal and spatial factors. However, this assumption is often wrong, primarily as a result of the same property that allows these pulses to be short—their broad spectral bandwidth. Angular dispersion, the best known source of such distortions, is everywhere, and the broader the pulse bandwidth the more distorted the pulse after an angularly dispersive element. Thus, in most practical cases, ultrashort pulses exhibit an interdependence of temporal (or spectral) and spatial (or angular) coordinates, referred to as spatio-temporal couplings (STCs).

The sources of STCs are ubiquitous. The most common source of STCs is the prisms and gratings used in pulse compressors for dispersion management and which are part of nearly every ultrashort-pulsed laser oscillator and amplifier. Pulse compressors function by purposely introducing STCs (angular dispersion) so that the path length of each color in the pulse is different in order to adjust the spectral phase. But, in the end, a successful pulse compressor must remove all of the couplings, which enforces strict alignment requirements on the device. Another simple example is the propagation

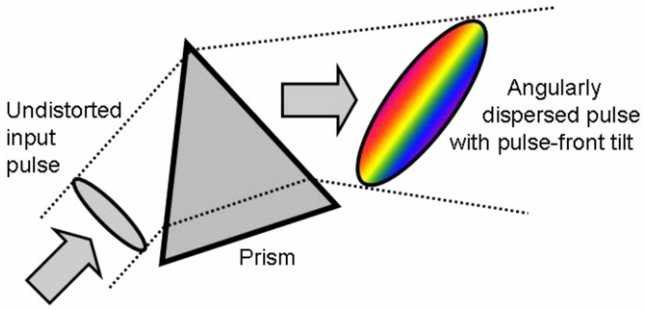

Figure 1. Propagation through a prism introduces STCs. Due to the dispersion of the prism's glass, the output beam exhibits angular dispersion and pulse-front tilt, which after propagation generates a third STC, spatial chirp.

of a pulse through a singlet lens, which results in a radially varying dispersion (spectral phase) due to the radially varying thickness of the glass [6]. Nonlinear optical interactions, such as nonlinear refraction and filamentation, can also introduce spatial and temporal couplings in light pulses.

While some STCs are well-known effects, others are still rather surprising. The best known STCs, angular dispersion, occurs when different spectral components of the pulse propagate in different directions, and is introduced by prisms, gratings and etalons. After some propagation, angular dispersion causes the spectral components to spatially separate, introducing another STC, spatial chirp (where the mean frequency varies with the transverse coordinate). The peak of the temporal intensity of the pulse can also vary with the transverse spatial coordinate if pulse-front tilt is present. The arrival time of the peak intensity may also depend on propagation direction, a lesser known effect called, for lack of a more interesting term, time versus angle. Figure 1 shows some of the more common couplings that result from propagation through a prism. Apart from these couplings in the electric field's intensity, the phase of ultrashort pulses may also (and very often does) exhibit couplings in the phase, giving rise to interesting phenomena such as wavefront rotation. There are eight first-order STCs in all and, in general, if a pulse has a coupling in one domain, it has at least two in every other Fourier domain, resulting in a total of seven and possibly even eight different coupling. Finally, they are generally not small effects, and when they are present, they can reduce the pulse intensity by a large factor.

The almost ubiquitous and non-negligible nature of STCs in ultrashort pulses makes them impossible to ignore. The significance of these effects largely depends on the application, and pulse parameters, and while STCs may be negligible in some cases, they are detrimental in others. Although STCs commonly result from misalignments and seem undesirable, they can, on the other hand, be viewed as an additional, controllable pulse–beam parameter and become quite useful. Regardless of the case, a proper understanding and characterization of these effects are paramount. As a result, in recent years STCs have received much interest from ultrafast researchers in many different fields. Here, we present an overview of some of this work.

First we will discuss the general characteristics of STCs, including their sources and mathematical representation in different domains. We will describe all the possible STCs and show how they are related to one another. To do this, we will present a general theoretical approach for describing first-order couplings and their interdependence, which can easily be extended to describe higher-order couplings. Next, we will focus on the measurement of STCs and review the different experimental methods, some of which can only measure particular couplings, while others can measure the full spatio-temporal profile of an ultrashort pulse. Finally, we will discuss how to avoid or utilize STCs.

2. Characteristics of pulses containing spatio-temporal couplings

2.1. Sources of STCs

Common components used in the generation and application of ultrashort laser pulses can become sources of STCs. With their broad bandwidths, ultrashort pulses quickly spread out in space and time when propagating in an angularly dispersive medium because each color in the pulse propagates at a different angle and group velocity. Pioneering work by Fork and Martinez [7–9] demonstrated that, regardless of its sign, angular dispersion always yields negative group delay dispersion (GDD), and hence can be used to compensate for the positive dispersion introduced by most materials in the visible and near-IR. This led to the now ubiquitous *pulse compressor* (see figure 2), which uses the angular dispersion introduced by prisms or gratings to remove positive group delay dispersion from pulses [10–12]. Analogous schemes employing imaging systems to reverse the sign of the GDD are also used as pulse stretchers in chirped-pulse amplification set-ups [12, 13].

As shown in figure 1, prisms and gratings introduce additional STCs, including pulse-front tilt and spatial chirp [11, 14, 15]. To avoid these distortions, pulse compressors are usually built using four dispersive elements (or two in a folded configuration) (figure 2), where the first angular disperser introduces the desired negative GDD and the last three are required to cancel out all of the STCs, leaving only the desired negative chirp at the output. Unfortunately, proper operation requires perfect alignment, for otherwise, residual STCs are found at the output of the pulse compressor [16, 17], and because such large amounts of them are required in order to achieve the required magnitude of negative GDD, residual STCs in an improperly aligned pulse compressor may still be significant.

Prisms and gratings are also used for pulse shaping (see figure 17). In this application, as in pulse compression, these elements are used to spatially separate and recombine the frequency components of the pulse, but here allowing the use of amplitude and/or phase masks in the Fourier plane, thereby obtaining the desired pulse shape [18–21]. The zero-dispersion 4f geometry [18, 21, 22] is designed so that, when no mask is used (and with perfect alignment), the output pulse's spatial and temporal shape is unchanged. While pulse compressors introduce STCs from misalignment, Fourier

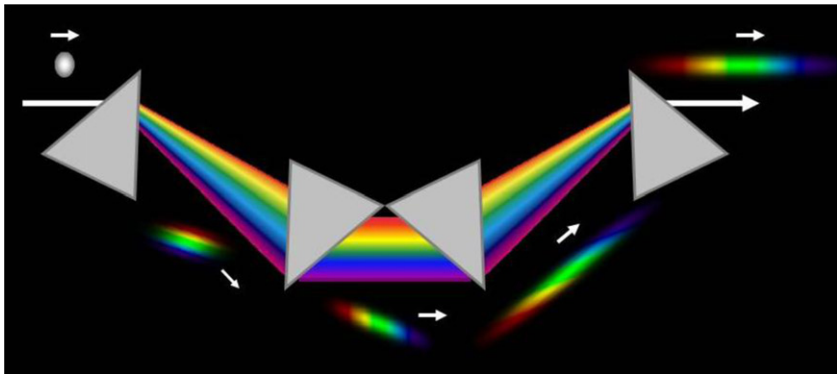

Figure 2. The four-prism (or grating) pulse compressor is a powerful device for dispersion control in ultrashort-pulsed laser set-ups. The pulse is shown in each stage of the device; note the significant amounts of spatial chirp and pulse-front tilt until the output.

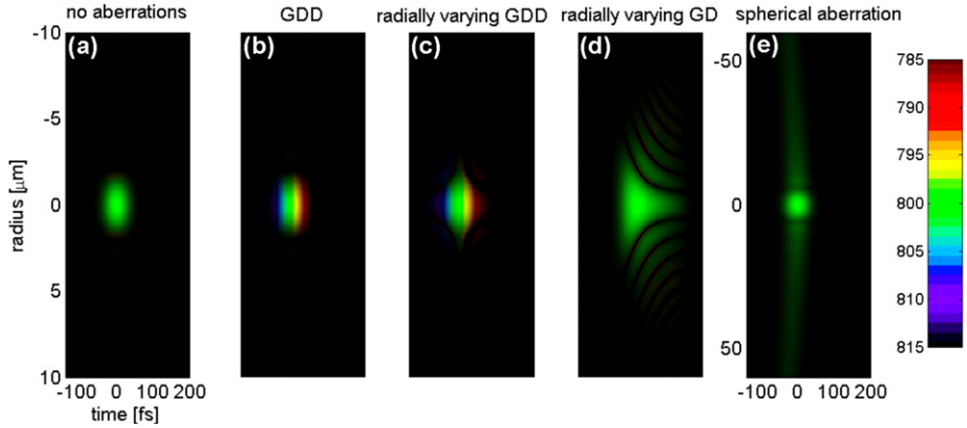

Figure 3. Simulations of a focused pulse from a 0.2 NA lens which was originally 30 fs long: (a) no aberrations. (b) Group delay dispersion. (c) Radially varying group delay dispersion. (d) Radially varying group delay. The curved pulse front causes the pulse to interfere with itself, resulting in the fringes seen in this plot. (e) Spherical aberration (note the different transverse scale in this plot).

synthesis pulse shapers introduce them even when perfectly aligned [21, 23, 24], mainly resulting from the diffraction, angular deviation and phase retardation caused by the spectral masks.

Lenses—one of the most common optical elements—are also a source of higher-order STCs. The couplings introduced by a lens are mainly due to the difference in the group and phase velocities of the lens material combined with its varying thickness, and any other lens aberrations. To first order, the radially varying thickness of the lens introduces a radially varying group delay, making the pulse front curved at the focus rather than flat (like the wavefront), which increases the effective pulse duration [6, 25–30]. This chromatic distortion can be eliminated by focusing with an achromatic lens [6, 28], but usually at the cost of additional temporal chirp in the pulse as these multi-element lenses are quite thick [31]. However, even if radially varying group delay is avoided, higher-order effects will still remain, such as radially varying GDD (and so on), which introduces (even in achromats!) a radially varying temporal chirp [28]. Achromatic aberrations such as spherical aberration also affect the spatio-temporal profile of a focused ultrashort pulse [29, 32], mainly because they contribute to the pulse-front curvature at the focus (because different parts of the beam are focused to slightly different planes), thus spreading the pulse in space–time. The types and magnitudes of STCs introduced by lenses depend on the properties of the lens and the pulse and are generally more serious for larger bandwidths and tighter foci (some nice guidelines are given in [29]). Figure 3 shows spatio-temporal plots of a 0.2 NA focus with different aberrations present, where the color in the plots is the instantaneous frequency.

Even the diffraction of ultrashort pulses off simple apertures, like a circular aperture, can lead to spatio-temporal structure. Diffraction off any circular boundary (an annular slit, circular aperture or a circular disc) results in an additional pulse that trails the main pulse front, called the boundary wave pulse, which is due to the interference of spherical waves emitted along the circular boundary [33, 34]. The right image in figure 4 shows an example (simulation) of a boundary wave pulse that was formed by propagating a collimated Gaussian beam with a 4 mm FWHM spot size through a 4 mm diameter hole. Boundary wave pulses can also appear at or near the focus if the lens aperture is smaller than the beam's full spatial extent, although focusing and lens aberrations can change its size and group velocity [26]. In the absence of aberrations, the additional pulse will be behind the main pulse in time (as in the

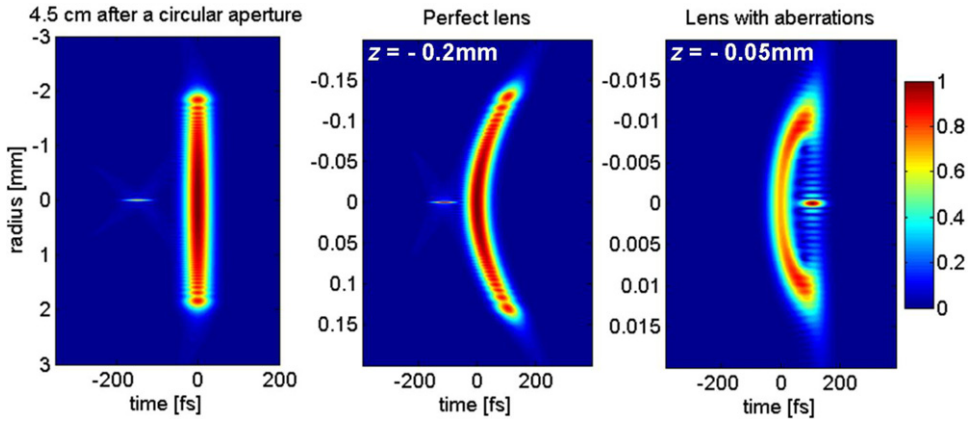

Figure 4. Boundary wave pulses: left: after a collimated pulse propagates through a circular aperture. Center: just before the focus of a perfect lens (NA = 0.5) with an aperture size equal to half of the beam's FWHM. Right: just before the focus of an (NA = 0.5) lens with spherical and chromatic aberrations, and an aperture width equal to the beam's FWHM.

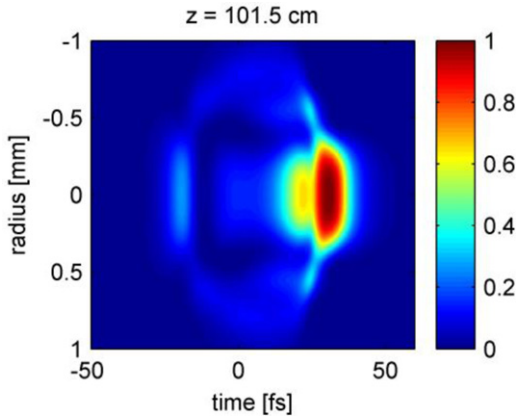

Figure 5. Simulation of the spatio-temporal intensity profile of an ultrashort pulse in a filament.

center image of figure 4) before the focus ($z < 0$) and ahead of the main pulse after the focus, and the two temporally overlap at the focus. Chromatic aberrations in the lens cause the boundary wave pulse to speed up so that it no longer temporally overlaps with the main pulse at the focus, but is instead ahead, so it is often called the forerunner pulse [26, 29, 35].

Nonlinear propagation of ultrashort pulses is another source of potentially complicated, higher-order spatio-temporal structures. The dependence of the nonlinear interaction on the pulse's intensity and phase couples the pulse's spatial features to the temporal features. A dramatic example is filamentation [36, 37]. Light filaments form when the self-focusing from Kerr lensing overcomes diffraction, leading to beam collapse and consequent photoionization. The process is highly dynamic and includes high-order nonlinear interactions [37–40] (see figure 5). These spatio-temporal dynamics play a leading role in the very useful effect of self-compression of laser pulses in a filament [41–43].

Due to the highly nonlinear behavior of gain media, laser cavities are another potential source of complicated spatio-temporal structures. Although such structures are much more complicated to model than those discussed above, some interesting aspects can be found in the literature (see, for example, [44, 45] and references therein).

2.2. Mathematical description of STCs

The potential complexity of STCs knows no bounds, and many different STCs can appear at the same time. As figure 1 shows, a prism (or a grating) introduces both angular dispersion and pulse-front tilt. This observation has even led to the widely quoted—but incomplete—conclusion that these two phenomena are equivalent [46–48], and which was later clarified when Zeek noted that simultaneous spatial and temporal chirp (even in the absence of angular dispersion) is another source of pulse-front tilt [49]. The existence of several distinct couplings and their interdependence somewhat complicates the description of the spatio-temporal evolution of ultrashort laser pulses.

Much of the confusion resulting from the coexistence of various STCs can be overcome by noting that each coupling may be present, but in a slightly different form, in multiple domains. The evolution of the electric field of an ultrashort pulse can be expressed in the time domain or equivalently (via Fourier transformation) in the frequency domain. Similarly, the field's spatial dependence can be described in the transverse spatial coordinate domain or the corresponding spatial frequency domain. When STCs are present, the pulse must be simultaneously described in at least two dimensions, so there are a total of four equivalent domains which can be used: (x, t), (x, ω), (k, ω) and (k, t) (where x is transverse position, t is time, ω is angular frequency and k is spatial frequency in the x direction). We will consider only one transverse Cartesian coordinate (x), as the generalization to include the others is straightforward. As a result, the intensity and phase couplings (along with the temporal/spectral parameters) in any one of these four domains suffice to completely describe the spatio-temporal evolution. The couplings in other domains are simply equivalent representations and their relationship to one another can be found by taking Fourier transforms.

Consider as an example pulse-front tilt, which is an intensity coupling in the (x, t) domain. By Fourier-transforming the field in this domain with respect to both time and position, one can obtain the field in the (k, ω) domain, where the intensity coupling yields angular dispersion [50]. By including the phase couplings, one can find a more general relationship, indicating that pulse-front tilt results from angular dispersion and/or simultaneous spatial and temporal chirp [49, 51].

2.3. Analytical approach for first-order couplings

The description of different STCs in each of the domains above allows for an intuitive representation of it. In fact, by using Gaussian profiles in time and space, analytical expressions can be found for the relations between first-order couplings [51]; and the physical consequence of each effect can be easily simulated for better understanding. Here we will summarize this approach, which was presented in detail in [51].

A linearly polarized ultrashort-pulsed laser beam can be described by the scalar electric field in space and time $E(x, y, z, t)$. Taking z as the propagation direction and x and y as the transverse coordinates, there will be only three independent degrees of freedom for the beam–pulse, because the electric field satisfies the wave equation given by

$$\left(\nabla^2 - \frac{1}{c^2}\frac{\partial^2}{\partial t^2}\right) E(x, y, z, t) = 0. \tag{1}$$

If one knows the electric field at a transverse plane $z = z_0$, the field at any other z plane can be found via Huygens' integral [52]. Here we will also work with only one transverse coordinate x and use scalar fields. A beam–pulse is free of STCs if the spatial and the temporal dependence of the electric field can be separated:

$$E(x, t) = E_x(x) E_t(t). \tag{2}$$

When the spatial and temporal dependences are coupled, the electric field cannot be separated as in equation (2) and, for a first-order coupling, the field becomes

$$E(x, t) \to E(x, t + \zeta x) \tag{3}$$

where ζ is the coupling parameter. Note that equation (3) can equivalently be written by adding a t dependence to x. This means that one can think of pulse-front tilt in two equivalent ways: as a transverse-position-dependent arrival time of the maximum intensity or alternatively as a time-dependent maximum in the transverse position intensity. This argument is also valid for the couplings in other domains, which will be addressed in more detail below.

In order to introduce an STC, we first write the complex temporal amplitude of an ultrashort pulse:

$$E(t) = \sqrt{I(t)}\exp[-\mathrm{i}\phi(t)] \tag{4}$$

where $I(t)$ is the intensity and $\phi(t)$ is the temporal phase. Assuming a Gaussian beam–pulse and temporal phase of up to second order (linear chirp), the electric field can be written, in a compact manner, as

$$E(x, t) \propto \exp\{\tilde{Q}_{xx}x^2 + 2\tilde{Q}_{xt}xt - \tilde{Q}_{tt}t^2\}. \tag{5}$$

This representation is also compatible with Kostenbauder ray-pulse matrices used to model dispersive optical systems [53]. The complex $\tilde{Q}$ coefficients correspond to physical parameters describing the evolution in space and time:

$$\tilde{Q}_{xx} = -\mathrm{i}\frac{\pi}{\lambda R(z)} - \frac{1}{w^2(z)} \qquad \tilde{Q}_{tt} = -\mathrm{i}\beta + \frac{1}{\tau^2} \tag{6}$$

where λ is the wavelength, R is the beam radius of curvature, w is the beam spot size, β is the chirp and τ is the pulse duration. The cross-term $\tilde{Q}_{xt}$ contains the STC information. Since the pulse intensity is the squared magnitude of the electric field, the real part of $\tilde{Q}_{xt}$ yields the position-dependent intensity arrival time, or the pulse-front tilt. The imaginary part, on the other hand, yields a time-and-position-dependent phase. Physically, this phase distortion causes the wavefront of the pulse to rotate in time, so it can be called 'wavefront rotation' (see a movie of this effect in [51]).

While the $\tilde{Q}_{xt}$ term describes the STC in the (x, t) domain in a mathematically convenient way, a normalized parameter would be preferable for comparison with experimental values. As mentioned above, the normalization can be done by including the x dependence on t (as in equation (3)) or vice versa. This is equivalent to rearranging equation (5) to write it in the form $\exp[(t + \zeta x)^2]$ or $\exp[(x + \varsigma t)^2]$, which indicates that the pulse-front tilt can be described by ζ (with units of time/position used in most experimental measurements [17]) as the real part of $\tilde{Q}_{xt}$ normalized by the pulse width; or equivalently by ς (with units of position/time) as the real part of $\tilde{Q}_{xt}$ normalized by the beam spot size (see figure 6). The ζ and ς parameters are related to each other (see [51] for details)

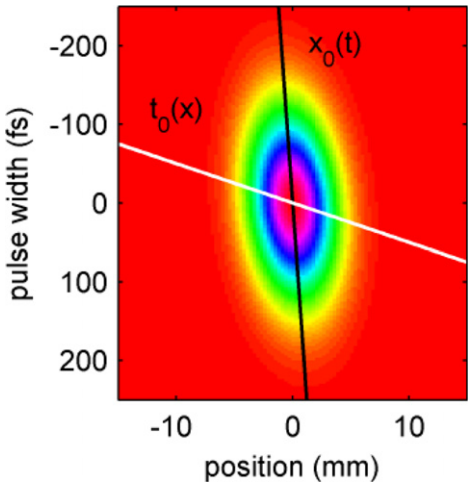

Figure 6. The intensity of a pulse with tilted front, plotted in position and time. The black line shows the beam center at each time, $x_0(t)$, while the white line shows the arrival time of intensity maxima for each position, $t_0(x)$. The inverse slope of the former yields $\varsigma = \mathrm{d}x_0/\mathrm{d}t$, while the slope of the latter yields $\zeta = \mathrm{d}t_0/\mathrm{d}x$.

by

$$\zeta = \frac{\varsigma}{\varsigma^2 + \frac{w_L^2}{\tau_G^2}}, \tag{7}$$

where w_L and τ_G are, respectively, the local spot size and global pulse width (see below for the definitions of local and global). The same principle was demonstrated earlier in the (x, ω) domain [54], including an experimental illustration. It was shown that the spatial chirp can be written as the frequency gradient (the variation in the peak frequency with position) or spatial dispersion (the variation in the peak position with frequency) and that the two are related by an equation equivalent to equation (7) [54].

While the normalization scheme above results in two mathematically equivalent expressions, for experimental considerations it is important to pay attention to the way the couplings are actually introduced. In the case of spatial chirp, the use of spatial dispersion [54] dictates $x \rightarrow x + \frac{dx_0}{d\omega}\omega$, which will make the beam larger in size when mapping each frequency to a different position. On the other hand, a frequency gradient means $\omega \rightarrow \omega + \frac{d\omega_0}{dx}x$ which will increase the frequency bandwidth. Since spatial chirp is most commonly introduced through linear optical systems, which rarely alter the bandwidth, spatial dispersion is more fundamental and so is preferred. Frequency gradient, on the other hand, should be calculated indirectly using the equivalent formula of equation (7) [54]. This consideration is analogous to the description of chirp in the time and frequency domains, where the frequency domain chirp parameter (group delay dispersion) is more fundamental than its time domain counterpart in a linear optical system.

As a result of these multiple definitions, the units and especially the magnitudes of STCs can be confusing (is 10 fs mm^{-1} a large or small amount of pulse-front tilt?), so it is more experimentally intuitive to define them in terms of dimensionless quantities, which can be used for non-Gaussian beams/pulses. This is done by normalizing the STC with respect to the two relevant beam/pulse widths, for example, for pulse-front tilt, both the beam width (w_G) and the pulse duration (τ_G) [55], as follows:

$$\rho_{xt} \equiv \frac{\int\int xtI(x,t)\,dx\,dt}{\int\int I(x,t)\,dx\,dt}\frac{1}{w_G\tau_G} = \frac{\tilde{Q}^R_{xt}}{\sqrt{-\tilde{Q}^R_{xx}\tilde{Q}^R_{tt}}}, \tag{8}$$

where the superscript R denotes the real part. This normalization has the advantage that the coefficient ρ is always between 1 and -1, and hence can easily show whether the coupling is 'large' or 'small'. The following reference gives some nice guidelines for 'acceptable' and 'unacceptable' values of ρ for different STCs [55].

Before using such a definition, however, it is important to realize that, even defining the widths (the beam spot size, pulse width, bandwidth and angular divergence) becomes subtle when an STC is involved. In the presence of pulse-front tilt, for example, the spot size at a given moment will be less than the spot size integrated over time. These two types of widths are defined as *local* and *global*, respectively. Using the root-mean-square definition, the local and global spot sizes are found to be

$$\Delta x_L(t) = \left[\frac{\int [x - x_0(t)]^2 I(x,t)\,dx}{\int I(x,t)\,dx}\right]^{1/2} = \left[-\frac{1}{4\tilde{Q}^R_{xx}}\right]^{1/2}$$
$$\Delta x_G = \left[\frac{\int\int x^2 I(x,t)\,dx\,dt}{\int\int I(x,t)\,dx\,dt}\right]^{1/2} = \frac{1}{2}\left[-\frac{\tilde{Q}^R_{tt}}{\tilde{Q}^R_{xx}\tilde{Q}^R_{tt} + \tilde{Q}^{R2}_{xt}}\right]^{1/2} \tag{9}$$

where $x_0(t)$ is the time-dependent beam center:

$$x_0(t) = \frac{\int xI(x,t)\,dx}{\int I(x,t)\,dx}. \tag{10}$$

Similarly, for the pulse duration, the widths are given by

$$\Delta t_L = \left[\frac{1}{4\tilde{Q}^R_{tt}}\right]^{1/2} \qquad \Delta t_G = \frac{1}{2}\left[\frac{\tilde{Q}^R_{xx}}{\tilde{Q}^R_{xx}\tilde{Q}^R_{tt} + \tilde{Q}^{R2}_{xt}}\right]^{1/2}. \tag{11}$$

It is important to distinguish between the local and global quantities. For instance, beam profiles are usually measured with slow detectors, which integrate the pulse over time; hence they yield the *global* beam spot sizes. Also, measuring the pulse duration of a small portion of the beam results in the local pulse duration, which can be significantly shorter than the global pulse length.

Having examined the STCs and their effects in detail in the (x, t) domain, it is now straightforward to extend the analysis to other domains, simply by Fourier (or inverse) transforming the electric field with respect to the proper variable:

$$E(x,\omega) = \frac{1}{2\pi}\int E(x,t)e^{-i\omega t}\,dt$$
$$E(k,\omega) = \frac{1}{2\pi}\int E(x,\omega)e^{-ikx}\,dx \tag{12}$$
$$E(k,t) = \int E(k,\omega)e^{i\omega t}\,d\omega.$$

For a Gaussian beam–pulse, the Fourier transforms in equations (12) can be evaluated analytically in each of these domains [56] resulting, in each case, in an electric field having the same form as equation (5). Consequently, the arguments above about the behavior of STCs in the (x, t) domain (normalization and definition of widths) can be easily generalized by replacing the parameters in equations (8) and (9) with their appropriate counterparts.

It is worthwhile noting that knowledge of the spatio-temporal field in the (x, t) domain (or in any one of the four domains) is sufficient to find the field in the other three domains. As a result, we can reach the following important conclusions that, to the first order: (i) there are a total of eight STCs (four intensity and four phase) and (ii) only two of these couplings are independent. In table 1, we list all of the first-order STCs.

Another advantage of this scheme is that direct analytical relations between STCs in different domains can be obtained. A complete table of formulae can be found in [51]. One of the results from this table can be written (with proper normalizations) as

pulse-front tilt = angular dispersion
+ temporal chirp × spatial chirp, (13)

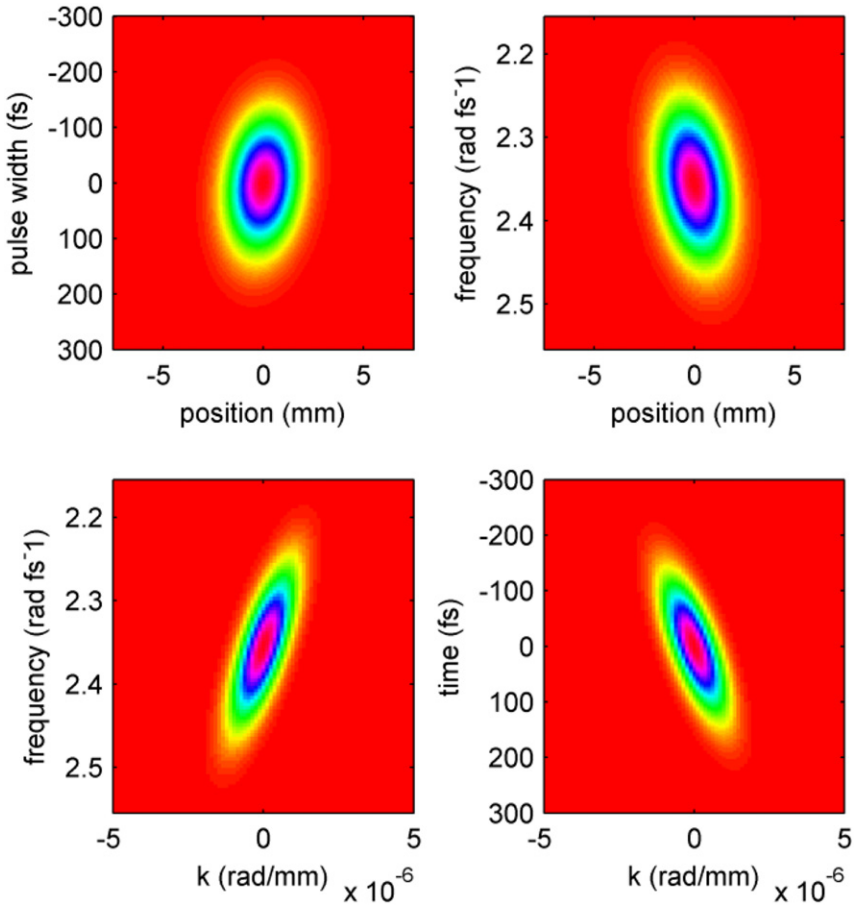

Figure 7. Intensity profiles in the (x, t), (x, ω), (k, ω) and (k, t) domains, resulting from a misaligned pulse compressor (parameters given in the text). The dimensionless coupling coefficients are: $\rho_{xt} = -0.16$, $\rho_{x\omega} = 0.26$, $\rho_{k\omega} = -0.71$ and $\rho_{kt} = 0.7$.

Table 1. Intensity and phase couplings in different domains.

Domain	Intensity coupling	Phase coupling
(x, t)	Pulse-front tilt	Wavefront rotation
(x, ω)	Spatial chirp	Wavefront tilt dispersion
(k, ω)	Angular dispersion	Angular spectral chirp
(k, t)	Time versus angle	Angular temporal chirp

which is equivalent to the results obtained in a case-specific study [49]. It is also interesting to note that the intensity coupling in any one domain yields a contribution to the phase coupling in the adjacent domain. The spatial chirp, for example, can be manifest in the time domain as wavefront rotation. This can be understood if we consider that spatial chirp causes the center frequency to increase (or decrease) across the beam, which in turn causes the phase to evolve faster (or slower) along the transverse axis, and thus the wavefronts (planes of constants phase) will rotate as time passes.

While it is very useful to find all eight STCs starting from two (one intensity and one phase in a given domain), it is experimentally more difficult to measure phase couplings (see about measurement methods in section 3) because most detectors and even considerably more sophisticated pulse measurement techniques are insensitive to this information. Fortunately, using the method above, it is possible to express the phase coupling in terms of the intensity coupling in the adjacent domain. Using the table of formulae in [51], once more we write

$$\text{wavefront rotation} = \frac{\text{spatial chirp}}{2} + \text{temporal chirp} \times \text{pulse-front tilt}, \tag{14}$$

again with proper normalizations. Analogous expressions can be found for the other phase STCs as well. The significance of equation (14) is that the phase STC, wavefront rotation, can be written in terms of spatial chirp and pulse-front tilt, two intensity couplings. This leads to an important conclusion that two intensity couplings suffice (along with the beam and pulse parameters) to retrieve the remaining six STCs.

In figure 7, we present a simulation of a first-order STC in a realistic scenario. We start with a pulse with a transform-limited duration of 20 fs FWHM and a collimated 2 mm waist size (beam divergence also affects the STC [11, 57], which is also accounted for in our approach since the radius of curvature is included in equation (6)). This pulse is then chirped by the introduction of 10^4 fs^2 group delay dispersion. In order to recompress this pulse, we simulate a four-prism pulse compressor, made with equilateral SF14 prisms, separated by 50 cm (between the first–second and third–fourth prisms, see figure 2). This compressor over-compensates the GDD by -1400 fs^2. Assuming that all prisms are used in the

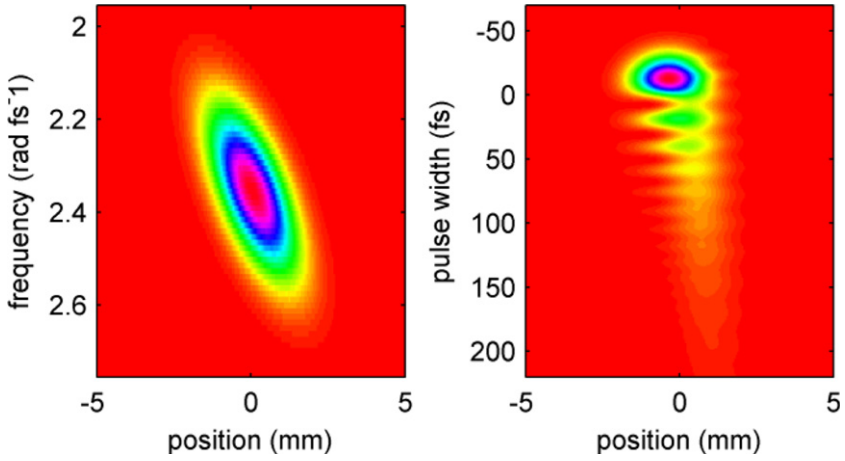

Figure 8. Intensity profiles in the (x, ω) and (x, t) domains for a spatially chirped pulse which has nonzero third-order spectral phase.

minimum-deviation configuration, except for the last, which is misaligned merely by 1°, we calculate the spatio-temporal intensity profiles 5 m after the pulse compressor. In figure 7, we display the intensity profiles in all four domains, which exhibit tilted ellipses, indicating the presence of intensity STCs. The dimensionless coupling parameters are indicated in the caption. Note that such a minute misalignment is sufficient to cause significant distortions.

2.4. Higher-order effects and more complicated profiles

In section 2.3, we described a general theory of first-order STCs of Gaussian pulses and beams. While the approximations made may appear restrictive, the approach can in principle be generalized to include arbitrary profiles and couplings of arbitrary orders. Once the complete spatio-temporal electric field of the pulse is defined in any one of the four domains, the fields in the other three can be found (typically numerically), allowing for a direct examination of the couplings. In figure 8, we simulate a pulse with a Gaussian spectrum, linear spatial chirp, but spectral phase up to the third order. Upon transformation to the (x, t) domain, we observe the interesting result that the satellite pulses resulting from the third-order spectral phase shift apart *spatially*, due to the pulse-front tilt resulting from simultaneous spatial and temporal chirp.

There are many types of nonlinear STC, some introduced by the higher-order angular dispersion of prisms and gratings, others by effects like lens aberrations. For example, the lowest-order chromatic aberration, or radially varying group delay, introduces an $x^2\omega$ phase coupling just after the lens which results in a quadratic pulse front (i.e. higher-order pulse-front tilt) [6]. Radially varying GDD comes about from an $x^2\omega^2$ phase term due to the varying thickness of the lens, which will make the local pulse duration vary with x. Lowest-order spherical aberrations are described by an $x^4\omega$ phase term, which produces a quartic pulse front after the lens. The following references give formulae for calculating these couplings from the lens, pulse and beam parameters [29, 32]. In many realistic cases, all of these couplings, as well as some higher-order ones, can be present in a focused ultrashort pulse. If the lens is placed after a misaligned pulse compressor, stretcher or pulse shaper, the linear couplings may be present as well. All of these common STCs make it easy for an ultrashort pulse to be very complicated.

3. Measurement of STCs

A major reason why spatio-temporal couplings in ultrafast laser beams have not been studied, removed and exploited much is probably the difficulty in measuring them. Indeed, the mere temporal characterization of an ultrashort laser pulse in the complete absence of STCs had already been a very challenging task itself until sophisticated techniques were developed, the most popular being frequency-resolved optical gating (FROG) [58]. Adding an entangled spatial dimension just makes the characterization problem even more difficult because the pulse's intensity and phase then need to be measured simultaneously in both space and time (or any equivalent set of domains). And many common STCs, like those from nonlinear propagation and lens aberrations, result in small temporal, spatial and/or spectral features, so high resolutions are often needed for these measurements.

In this section, we review the state of the art of techniques for measuring spatio-temporal couplings in ultrashort laser pulses. We will begin with the measurement of one particular type of STC, and then move on to discuss more general and comprehensive techniques capable of measuring the full spatio-temporal electric field (intensity and phase). As we have shown in section 2, with knowledge of the spatio-temporal electric field in one domain, we can easily deduce the form of the field in all three other domains with simple Fourier transforms.

3.1. Measurement of an individual STC

3.1.1. Spatial chirp. Of all the types of STC, spatial chirp is probably the easiest to measure [54]. A spectrometer provides the spectral resolution necessary for the measurement. And if the spectrometer has an iris aperture as its entrance (e.g. through an optical fiber), taking spectra while translating

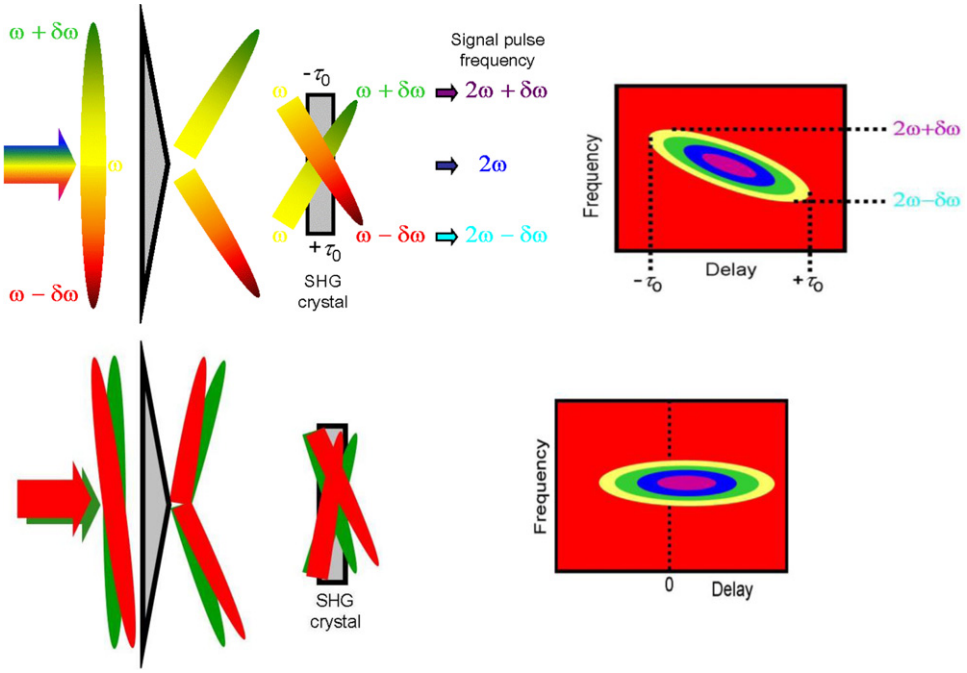

Figure 9. Spatial chirp tilts the trace (above) and pulse-front tilt translates the trace in delay (below) in GRENOUILLE measurements. This allows GRENOUILLE to measure these distortions easily and without modification to the apparatus.

the entrance iris on the x–y plane provides an $I(x, y, \omega)$ profile. More conveniently, an imaging spectrometer with an entrance slit (along the x direction) and a 2D detector yields $I(x, \omega)$ directly at its image plane on a single-shot basis without the need for scanning. From such measurements, both the spatial dispersion and the frequency gradient (as well as any higher-order $x\omega$ couplings in the intensity) can be extracted following the definitions described in section 2.3.

It was recently discovered that a single-shot second-harmonic-generation (SHG) FROG device (and its simpler version GRENOUILLE) also measures linear spatial chirp, as illustrated in figure 9 [59]. Because a single-shot SHG FROG device mixes the frequencies of different spatial parts of the input beam along a line focus in order to create delay resolution, spatial chirp in the input beam will result in a tilt of the measured, otherwise symmetric, FROG trace in the τ–ω plane. The amount of tilt can be quantitatively measured and used to deduce spatial chirp. It is interesting to note that a FROG measurement yields the frequency gradient parameter directly; in order to obtain the spatial dispersion parameter, one can use the equivalent of equation (7) [54]. The great advantage of using single-shot FROG or GRENOUILLE to measure spatial chirp is its experimental simplicity. A typical ultrafast laser lab probably already uses a FROG to measure the temporal profile of their pulses, so the benefit of spatial chirp detection comes at no additional experimental effort.

3.1.2. Pulse-front tilt. The second important class of STC measurement techniques are those that measure pulse-front tilt. As discussed above, two different types of pulse-front tilt are commonly found in ultrashort laser pulses: linear pulse-front tilt resulting from angular dispersion or spatial and temporal chirp, and radially varying group delay from chromatic aberrations which results in a curved pulse front. We will discuss the measurement of these two types of pulse-front tilt separately.

3.1.2.1. Linear pulse-front tilt (and angular dispersion). A large number of devices in ultrafast optics are based on interferometers. Depending on the spatial parity of the beams in the two arms of the interferometer (which in turn depends on its geometrical configuration), signatures of pulse-front tilt can be embedded in the measurement, which can then be used to determine the amount of pulse-front tilt.

A. Interferometric field autocorrelation. The earliest techniques developed to measure linear pulse-front tilt used linear spatial interferometry. In these techniques [60, 61], the beam in one arm of a standard Michelson interferometer is spatially flipped (e.g. by using different numbers of reflections in the two arms). The output beams from the two arms are then crossed at a small angle and a CCD camera captures spatial interference fringes where they overlap. When the path length difference between the two arms is varied, a packet of interference fringes can be observed to appear from one side of the beam, move to the center when the path lengths of the two arms are the same and then disappear at the other side of the beam. Thus, by measuring the center position of the fringe packet as a function of relative delay, one can calculate the value of the pulse-front tilt.

However, there is an important caveat in the interpretation of the measurement results of this method. As it is based on linear interference, it does not actually measure all sources of pulse-front tilt. In fact, an ultrashort pulse is not even needed for this technique; a broadband light source having an equivalent coherence length will yield the same interference fringe packet. In order to form interference, this technique

assumes that different parts of the beam have the same spectral content, so it cannot measure the type of pulse-front tilt resulting from the coexistence of spatial chirp and temporal chirp [49]. What is measured is actually only the pulse-front tilt caused by angular dispersion.

Angular dispersion can also be measured by combining an imaging spectrometer with an inverted-beam Michelson interferometer [57]. A spectrally resolved spatial interference pattern is recorded on the image plane of the spectrometer, which contains information about the angular dispersion in the spectral dependence of the spatial fringe spacing. An angular chirp measurement resolution of 0.2 μrad nm^{-1} has been demonstrated with this technique.

B. Single-shot intensity autocorrelators. Another class of pulse-front tilt measurement techniques is based on the single-shot noncollinear intensity autocorrelator, which is a slightly angle-detuned interferometer with an SHG crystal at the beam crossing point [62]. A delay-varied SHG autocorrelation signal is generated along the direction of beam crossing, allowing for temporal characterization of the pulse. As with the spatial interferometer, if the two interacting beams have different spatial parity, pulse-front tilt can leave a signature in the measurement result. Being nonlinear optical in nature, these techniques measure the true pulse-front tilt, as the SHG signal is generated only where the two pulse fronts meet.

In most single-shot autocorrelators, the beam is line-focused at the SHG crystal in order to obtain a high SHG efficiency. With pulse-front tilt in the direction of the line focus, a usual non-inverted-beam Michelson-type autocorrelator produces an undistorted autocorrelation of the pulse, while an inverted-beam autocorrelator will produce an autocorrelation with a different width than the autocorrelation width of a spatio-temporal-coupling-free pulse [62]. Unfortunately, it is difficult to quantify the pulse-front tilt directly from such a comparison.

It is better to send an unfocused beam through a two-dimensional single-shot autocorrelator. It happens that, if the beam is spatially inverted in one arm of the autocorrelator in the plane perpendicular to that of beam crossing, the pulse-front tilt in the parity-inversion plane will cause a tilt in the spatial distribution of the SHG signal [62–64]. This tilt can then be quantified to determine the pulse-front tilt. Devices based on this principle are commercially available as 'tilted-pulse-front autocorrelators'.

C. GRENOUILLE. It might be a little surprising to note that even a beam geometry without inversion can also be used to measure pulse-front tilt. This is the case with GRENOUILLE, the simplified version of a single-shot FROG device [65]. It is found that, for simple geometrical reasons, pulse-front tilt along the beam-crossing direction in a GRENOUILLE causes a shift of the measured trace along the direction of beam crossing [17]. Therefore, the delay-center shift of the measured GRENOUILLE trace can be measured and used to calculate the pulse-front tilt in the beam. As in the case of the spatial chirp measurement, this feature comes with no modification to the GRENOUILLE device at all.

3.1.2.2. Curved pulse-front measurements. In many experiments, laser pulse fronts are distorted, but not in a linear fashion. One important example is the curved pulse front of a focused ultrashort pulse, which is the result of the chromatic aberration in the focusing lens. Some techniques have been developed to characterize such curved pulse fronts.

Most such curved pulse-front measurement techniques operate by the same principle as an interferometer or an intensity autocorrelator described in section 3.1.2.1. However, instead of overlapping two replicas of the same beam with different spatial parities, the interference or cross-correlation with a flat-pulse-front reference beam is used. When measuring the pulse front of a focused ultrashort pulse, a beam is usually passed twice through a lens under test, focused and recollimated, doubling the pulse-front curvature in the process, and then is allowed to interfere or correlate with a plane-wave reference beam.

The linear interference version of this technique is also known as light-in-flight holography [66] when an ultrashort pulse is involved. Although a linear interferometer, any light source with a comparable coherence length can be used for this measurement. A nonlinear optical crystal can instead be placed at the output of the interferometer to make an intensity cross-correlator [29, 67], which measures the true curved pulse front. A higher temporal resolution can be achieved when a short reference pulse is used for the cross-correlation.

Such measurements have been extensively used to characterize the curved pulse front of focused ultrashort pulses. The agreement between the measurement and calculation results was generally good.

3.2. Full spatio-temporal electric field measurements

Whereas the characterization of one or two spatio-temporal coupling parameters may suffice in some applications, in many others such a simple description falls short. This is especially true when the pulse bandwidth is broad, the spectrum and/or phase are complicated, or the spatio-temporal coupling is not linear. The ultimate measurement in such cases is that of the full intensity and phase of the complex spatio-temporal electric field.

It is fundamentally sufficient to measure the complex electric field in any one of the four spatio-temporal domains; the expressions in the three other domains can simply be obtained by performing Fourier transforms. Also, due to the wave equation, a propagating electromagnetic field has only three degrees of freedom. Specifically, in order to know the electric field in the full space–time, one need only determine the spatio-temporal field at one longitudinal coordinate z_0. Propagating to all other values of z can be simply achieved by applying Huygens' integral. Thus, in all the discussions below, we will only concern ourselves with the measurement of the electric field at one longitudinal plane.

Techniques in this category are often straightforward extensions of well-established temporal pulse characterization techniques—FROG, SPIDER or spectral interferometry. Some exceptions are also summarized.

3.2.1. Spatially resolved spectral interferometry and SPIDER. Spectral interferometry is a highly sensitive linear temporal

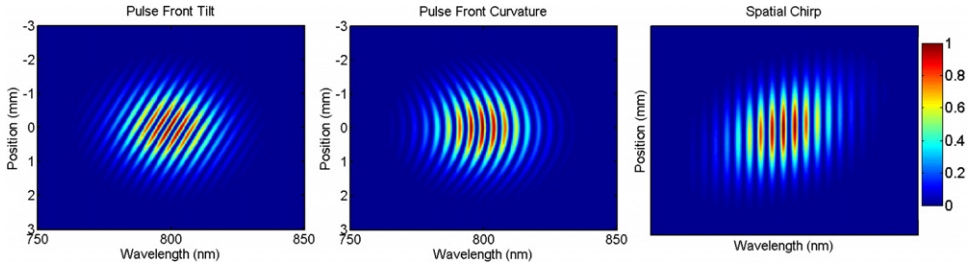

Figure 10. Spatially resolved spectral interferograms using a transform-limited reference pulse that is free of STCs when three different STC are present in the unknown pulse. Left: pulse-front tilt. Center: pulse-front curvature, such as that from chromatic aberration. Right: spatial chirp. The spectral fringes are due to the delay between the reference and unknown pulses, which is purposely introduced so that the Fourier filtering algorithm can be used to reconstruct the spatio-spectral electric field from the interferogram.

pulse characterization technique, in which the pulse to be characterized is combined with a known reference pulse with a certain relative delay introduced between them. This results in an interference fringe pattern in which the spectral phase difference between the interfering pulses becomes the phase of the spectral fringes. Combining this information with the spectrum and the spectral phase of the reference pulse (which must be known), the spectrum and spectral phase of an unknown pulse can be completely characterized. The most common and reliable algorithm for extracting the unknown field from the fringe pattern is Fourier transform spectral interferometry [68–70]. A major limitation of this method, however, is the requirement to have a well-characterized reference beam, which must include all frequency components present in the beam to be characterized, in order to form interference fringes at all the wavelengths of interest. Also, the unknown and reference pulses must be separated by approximately five pulse lengths in order to generate the spectral fringes required for the inversion algorithm, which has the significant disadvantage of significantly underutilizing the spectrometer resolution.

SPIDER is essentially a self-referenced version of spectral interferometry, in which both pulses are upconverted in a sum-frequency generation (SFG) crystal with a small frequency shear between them. Thus the derivative of the spectral phase (group delay) of the unknown pulse becomes the phase of the spectral fringes, which, along with an independent measurement of the spectrum, can be extracted to complete the temporal characterization of the pulse, provided that the time separation between the two pulses is known with very high accuracy [71]. Fourier filtering is also usually used for the reconstruction in SPIDER.

Because SPIDER and spectral interferometry are one-dimensional measurements, requiring only a linear array detector, the inclusion of an additional spatial dimension is rather straightforward by employing a imaging spectrometer and a 2D detector, like in the apparatus described earlier for the measurement of spatial chirp. For spatially resolved spectral interferometry, a temporally (spectrally) and spatially characterized reference beam is used so that the difference in the phases of the two beams can be extracted from the spatio-spectral interference pattern recorded on the 2D detector, which can be used to reconstruct the spatio-temporal electric field of the unknown pulse [72, 73]. Note that the same Fourier transform algorithm can also be used in the two-dimensional case to extract the unknown field, except that the Fourier transform must be taken for each value of x. As in the one-dimensional case, a pre-characterized reference pulse containing the spectrum of the unknown pulse must be used and, moreover, in the spatially resolved case, it must also spatially overlap with the unknown pulse. Spatially resolved spectral interferometry has been useful for several applications such as studying lens aberrations [74, 75] and self-focusing in transparent media [76, 77]. Figure 10 shows examples of spatially resolved spectral interferograms for three different STCs.

Because SPIDER is a self-referenced version of spectral interferometry, it can in principle also benefit from the same addition of one spatial dimension. However, there is another subtlety to be noted. Owing to its self-referencing nature, a spatially resolved SPIDER, which simply uses an imaging spectrometer to measure the spectral interferogram at each spatial position along one beam dimension [78], can determine most features of the spatio-temporal field. But it does not yield the spatial phase of the beam and the spatially varying group delay (the arrival time at each position or pulse front). In order to obtain the full information of the spatio-spectral phase, both spatial and spectral shearings should be present. Spatial shearing can be achieved by overlapping two spatially shifted beams on the 2D detector, while maintaining a small angle between their propagation directions, thus creating a carrier spatial modulation [50, 79]. The same algorithm for extracting the spectral phase can be used in the spatial domain.

Obviously, only one spatial dimension can be included in this type of method because the other spatial dimension is used for mapping wavelength onto position to measure the spectrum. But the field's dependence on the other transverse dimension can be measured by scanning a slit in that direction.

3.2.2. Spectrally resolved spatial interference. As mentioned above, an important practical limitation of the usual collinear spectral interferometry (and SPIDER) is that high spectrometer resolution is required, much of which is lost in the reconstruction algorithm [68, 80]. This is due to the fact that, in order to extract the spectral phase in the Fourier filtering algorithm, one needs to be able to separate the interference term from the DC component in the Fourier transform of

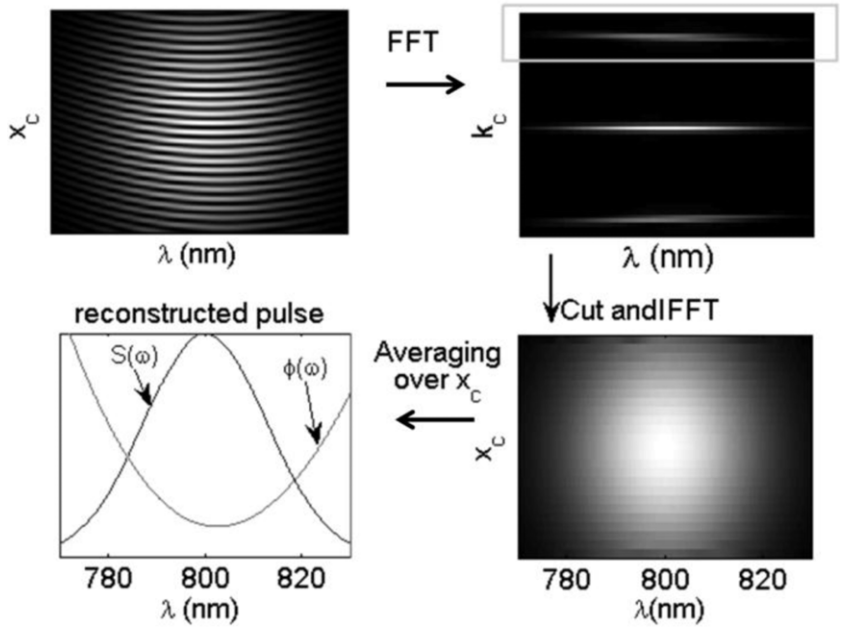

Figure 11. SEA TADPOLE retrieval. The top left image is a typical interferogram, which is Fourier-transformed from the λ–x_c to the λ–k_c domain where only one sideband is kept. This sideband is then inverse-Fourier-transformed back to the λ–x domain. The result is then averaged over x_c and the reference pulse is divided out in order to isolate the intensity and phase of the unknown pulse.

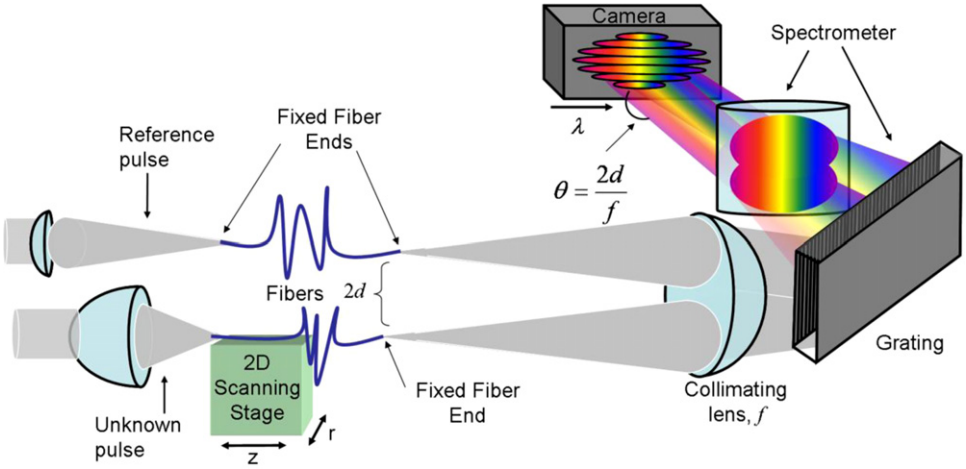

Figure 12. SEA TADPOLE experimental set-up. A reference pulse and an unknown pulse are coupled into two single-mode fibers with approximately equal lengths. At the other end of the fibers, the diverging beams are collimated using a spherical lens (f). After propagating a distance f, the collimated beams cross and interfere, and a camera is placed at this point to record the interference. In the other dimension, a grating and a cylindrical lens map wavelength onto the camera's horizontal axis x_c.

the interferogram. This requires that the interference fringe (carrier) spacing be smaller than the smallest feature in the signal spectrum, and so the spectrometer should have a resolution several times higher than that needed to resolve the smallest spectral feature in the unknown pulse.

It was later realized that, by temporally overlapping and crossing two beams at a small angle at the entrance slit of an imaging spectrometer to create a spatial carrier modulation, one can circumvent this problem and use the full resolution of the spectrometer to measure the unknown pulse. The Fourier filtering to extract the unknown pulse from the fringe pattern can be performed analogously to that in spectral interferometry, but instead along the spatial dimension, where the crossing angle plays the role of the delay [81]. This is illustrated in figure 11. Pulse characterization in this fashion has been suggested by [82] and Geindre *et al* [81], and systematically studied, simplified and developed as a generic pulse measurement technique (named SEA TADPOLE) by Bowlan *et al* [83]. The SEA TADPOLE experimental set-up is shown in figure 12. This method has also been applied to SPIDER to achieve the same spectral resolution benefits (named SEA SPIDER) by Kosik *et al* [84].

Though spectrally resolved spatial interferometry is more commonly used to measure just the temporal electric field with high spectral resolution, because it is two-dimensional, the spatio-spectral field of the unknown pulses is present in

the interferogram and can be extracted by the Fourier filtering algorithm. Just as spectral resolution is lost due to Fourier filtering along the frequency axis in spectral interferometry, in spectrally resolved spatial interferometry, some spatial resolution will be lost. But in the case of SEA TADPOLE, the use of fibers as the entrance conduits for the beam into the device results in the loss of the pulse's spatial information, and scanning of the fiber (see section 3.2.3) is necessary to measure the spatio-temporal field.

3.2.3. Scanning field measurements. Whereas the two methods described above can only measure a spatio-temporal field with one spatial dimension, full 2D spatial resolution can be achieved by scanning a smaller aperture across the beam and measuring the electric field of that sampled by the aperture. A single-mode fiber naturally acts as an aperture, sampling the electric field within its mode area. Its mode size can be as small as a few microns, enough to measure the field at a focus, which is important for many applications. In contrast, spatially resolved spectral interferometry can only measure recollimated beams, in which case information about the field at the focus can only be indirectly obtained, leaving it susceptible to apparatus misalignment [73, 74].

The electric field sampled through the aperture will then need to be measured temporally or spectrally resolved. Furthermore, in order to characterize the full spatio-temporal phase, it is important for the location-specific pulse measurement to preserve the 'absolute' temporal/spectral phase—in this case actually the spatial phase—in order to be able to stitch the measurement results together in a 3D fashion. In this regard, self-referenced FROG and SPIDER measurements are not sufficient, while spectral interferometry with a reference pulse is.

SEA TADPOLE uses a pair of single-mode fibers, one for sampling a known reference pulse (usually the beam before entering an optical system under test) and the other for scanning the field of the beam of interest, and is therefore ideally suited for this task. Figure 12 shows a schematic of scanning SEA TADPOLE. It has been demonstrated to work very well for high spatial and high spectral resolution characterization of a 3D spatio-temporal electric field, including focused electric fields, and Bessel-X pulses, with remarkable success [85–87]. When the single-mode fibers do not offer enough spatial resolution, fiber NSOM probes can instead be used to achieve sub-wavelength resolution [87]. Given its good performance and design simplicity, it is clearly the method of choice for full-3D spatio-temporal electric field characterization, whenever a suitable pre-characterized reference pulse is available, or when only the performance or distortion of a linear optical system (such as a dispersive medium or a pulse shaper) is of interest. Figure 13 (top) shows a scanning SEA TADPOLE measurement from a 0.44 NA lens which has a lot of chromatic aberrations, a little spherical aberration, and the additional pulse is due to diffraction off of the lens' aperture. The additional pulse or the 'forerunner' pulse is 500 nm is size, and so a 500 nm NSOM probe was used to make this measurement. The simulations shown below the measurements are to confirm their accuracy and use the method described in this [35].

3.2.4. Digital holography. Rather than adding spatial dimensions to a temporal pulse measurement technique, a different route to the full spatio-temporal characterization of an electric field involves extending a spatial field measurement technique into the time (frequency) domain.

The analog of spectral interferometry in the spatial domain is holography, in which the beam of interest is overlapped with a flat-wavefront reference beam at a small angle, and the resulting spatial interference fringes are recorded, which contain the difference of the spatial phases of the two beams [88]. Gabolde *et al* have developed a technique based on digital holography, in which they send a portion of the beam through a small pinhole and a narrowband frequency filter to create a quasi-monochromatic flat-wavefront reference beam [89]. Interfering the reference beam and the beam under investigation creates a digital hologram on the CCD detector at the narrowband filter's transmission wavelength. A series of measurements are made at different wavelengths across the signal spectrum. By applying the digital holography inversion algorithm, which is usually also Fourier filtered, one can obtain the spatial intensity and phase profiles at all the test wavelengths. A final FROG measurement is made to determine the spectral phase profile of the pulse, which links the holographic spatial phase profiles together. At the end of the measurement, a full 3D spatio-temporal intensity and phase profile of the beam is obtained.

A clever single-shot implementation, dubbed STRIPED FISH, was later demonstrated, using a low-resolution 2D diffraction grating and a large 2D CCD detector [90]. As shown in figure 14, the 2D diffraction grating creates a 2D array of replicas of the slightly crossing signal and reference beams, each beamlet pair emerging at a different angle. The beamlet array passes through a narrowband interference filter tilted at a small angle; the filter's transmission wavelength varies with the incidence angle, resulting in wavelength variation in the filter's tilting plane. Each beamlet pair in the 2D array overlap and interfere in a different section of the large CCD detector, allowing the simultaneous recording of the holograms at difference wavelengths. This single-shot design has been tested and demonstrated to work remarkably well with spatio-temporally distorted beams. An example of STRIPED FISH measurement of a pulse containing spatial chirp is shown in figure 15.

3.2.5. Other methods. Just as in the case of temporal or spatial characterization of an optical field, it is difficult to place all existing techniques into predefined boxes. For the sake of completeness, we will mention some other techniques not categorized in the previous discussions.

One technique, called CROAK [91], is based on a pair of spatially resolved spectral measurements in both the near- and far-fields and another FROG measurement of the temporal field. There is no analytical formula for the retrieval of the spatio-temporal field. Rather, a Gerchberg–Saxton algorithm is used to iteratively retrieve the spatial phase that yields the numerical evolution of the spatial spectra from the near-field to the far-field, which is combined with the FROG-retrieved spectral phase to construct the spatio-temporal phase. This

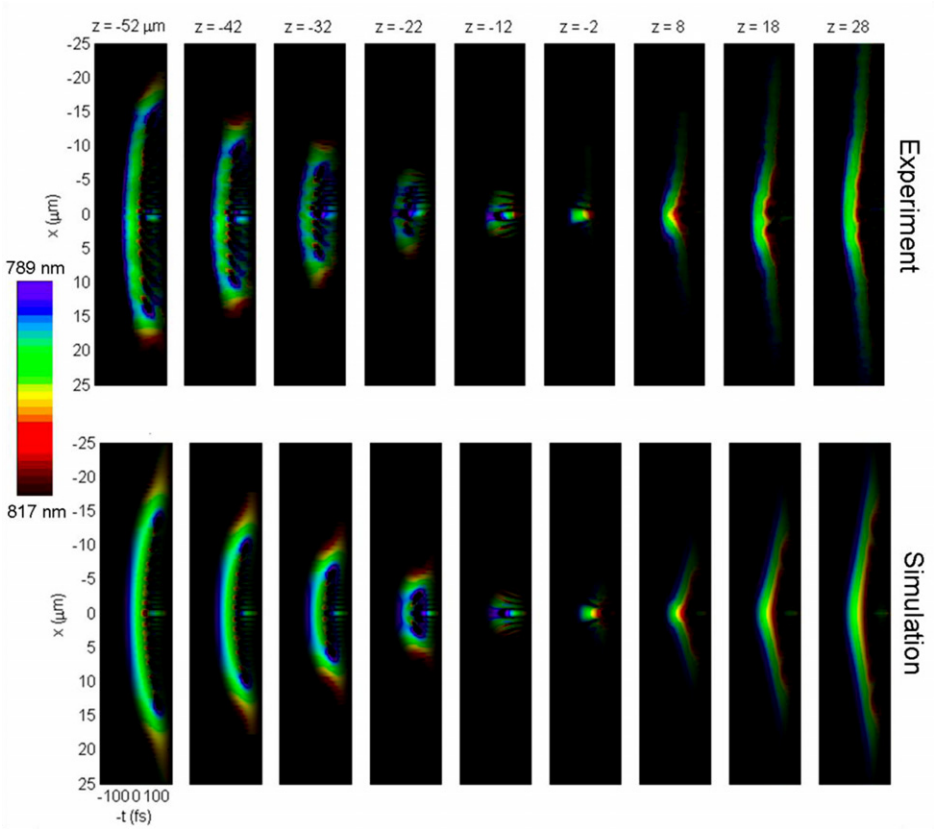

Figure 13. $E(x, z, t)$ in the focal region of an aspherical lens measured by scanning SEA TADPOLE. The experimental results are displayed in the top plots and the simulations are shown in the bottom plots. Each box displays the amplitude of the electric field versus x and $-t$ at a distance z from the geometric focus. The color represents the instantaneous frequency, which shows that the redder colors are ahead of the bluer colors due to material dispersion. Several STCs are simultaneously present in this focusing pulse giving it a very complex spatio-temporal field: diffraction off of the lens aperture results in the forerunner pulse, chromatic aberrations make the color vary with x and z, and the additional pulse (the forerunner pulse) is ahead in time, spherical aberrations make the forerunner pulse brighter, and material dispersion results in some temporal chirp or variation of the pulse's color with t. This data was taken from [87].

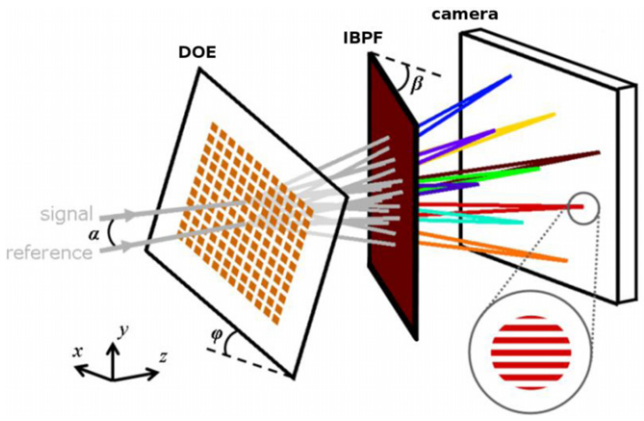

Figure 14. Three-dimensional view of STRIPED FISH. The signal and reference pulses are crossed at a small vertical angle α. The diffractive optical element (DOE) is rotated by an angle φ about the z axis and the interference bandpass filter (IBPF) is rotated by an angle β about the y axis. The inset shows one of the spatial interferograms ('digital holograms') captured by the digital camera.

method has been demonstrated to work on a simple one spatial dimension linearly coupled spatio-temporal field. However, its performance in more complicated situations has not been investigated.

There are also techniques based on the well-known Shack–Hartmann wavefront sensors, which detect local k-vectors in a beam. The first such technique was developed by Grunwald *et al*, in which a collinear intensity autocorrelator is combined with a Shack–Hartmann wavefront sensor [92]. In this technique, spatially resolved collinear interferometric autocorrelation traces are measured along with the local wavefront normals.

A further extension of this technique, called shackled FROG [93, 94], combines the Shack–Hartmann sensor with a FROG measurement performed at the center of the beam. The Shack–Hartmann wavefront measurements can be conducted at a series of distinct wavelengths within the pulse bandwidth or, in the case of one spatial dimension, on the focal plane of an imaging spectrometer. The FROG measurement serves to link all the phase measurements together. The shackled FROG technique has been successfully applied to measure the spatio-temporal structure in a tilted-pulse-front beam and a Bessel-X pulse.

Finally, an interesting technique based on scanning near-field microscopy has been developed [95, 96]. In this technique, a near-field probe is brought to the surface of a waveguide, sampling the local evanescent wave, which carries the amplitude and phase information of the propagating field.

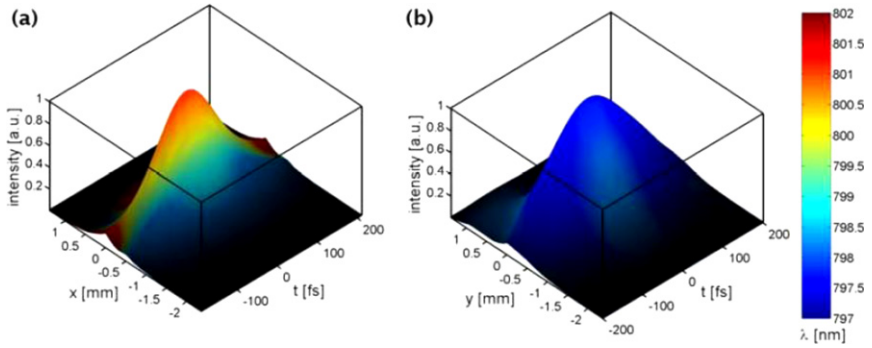

Figure 15. (a) x–t slice of the measured electric field $E(x, y, t)$ of a pulse with spatial chirp, temporal chirp and pulse-front tilt. The vertical axis shows the electric field intensity $|E(x, t)|^2$ and the color shows the instantaneous wavelength derived from the phase $\varphi(x, t)$. The spatial gradient of color shows the spatial chirp along the x direction. (b) y–t slice of the same measured electric field. No spatial chirp is present along the y direction, as expected.

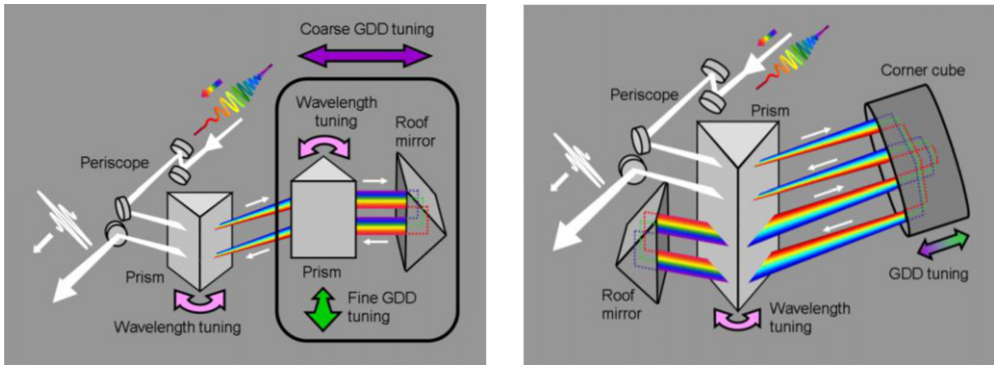

Figure 16. Two-prism (left) and single-prism (right) pulse compressors.

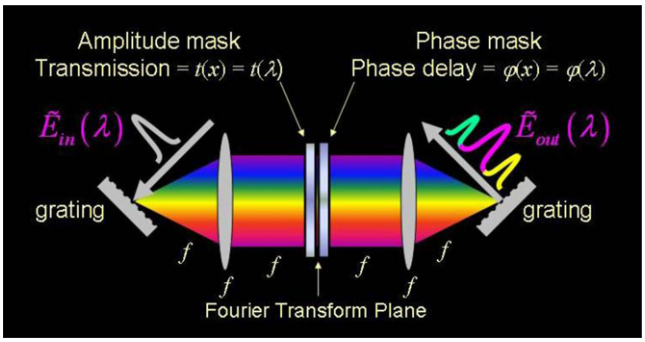

Figure 17. Standard 4f pulse shaper and spatio-temporal pulse shaper.

The output from the probe is then mixed interferometrically with a reference field, and a photodetector measures the modulation formed by interference. The near-field probe can be scanned with sub-wavelength resolution, producing a spatial map of electric field on the surface of the sample, whose Fourier transform is exactly the wavevector (k-space) distribution. The delay between the probe and the reference pulses can also be varied. Using this technique, one can track the evolution of the waveguide propagating mode in both k-space and time, uncovering a wealth of propagation dynamics in photonic crystal structures.

4. Effects and applications of STCs

Spatio-temporal couplings of an ultrafast laser beam are a rich phenomenon. On the one hand, they greatly complicate dealing with laser pulses, and for this reason, they are carefully avoided in many experiments. On the other hand, the ability to manipulate the pulse's spatio-temporal couplings provides a new degree of freedom in exploiting a laser pulse, which is very welcome in many tightly constrained experiments that demand optimal interaction of pulses. Indeed, they correspond to the information present in a pulse.

Whether to avoid them or to exploit them, the ultrafast scientist needs to quantitatively understand how spatio-temporal couplings are generated, how they evolve in an optical system and how they can affect experimental results in various situations. In this section, we will review some interesting spatio-temporal effects and their applications in various experiments.

4.1. Sources and avoidance of STCs

As mentioned previously, in many cases, STCs in ultrashort laser pulses result from misalignments of dispersion management devices, such as pulse compressors/stretchers which are composed of prisms and gratings. The commonly used four-prism (grating) compressor/stretcher design imposes strict alignment conditions to avoid residual STCs at the

output. As shown in the simulation results in figure 7, minute misalignments in prism angle can yield significant distortions. An elegant way of relaxing this tight alignment constraint is to use a single prism and corner cube [97]. This design exploits the fact that precision corner cubes not only return the beam parallel (to within a few arcseconds) to the incoming direction with a very high accuracy, but also they invert the beam image. In the configuration shown in figure 16, a corner cube after the first prism can be used to fold the beam and send it through the first prism for the second pass. Next, a simple roof mirror can send the beam back through the same prism again, at a different height. The last reflection through the corner cube and transmission through the prism completes the single-prism pulse compressor, equivalent to a four-prism design. Because of the involvement of a corner cube, the alignment constraints are significantly reduced. This single-prism pulse compressor is also more compact and much easier to tune for another laser center wavelength.

Another device that can introduce undesirable spatio-temporal couplings in a laser beam is the 4f pulse shaper [21]. Like a grating-pair pulse compressor, its very functionality relies first on the generation of spatio-temporal coupling—the input beam is spectrally dispersed on the Fourier plane, where a mask is used to modulate the spectral intensity and phase. The modulated frequency components are then synthesized back at the output, where the spatio-temporal coupling introduced in the Fourier plane should be exactly reversed and removed. However, in practice, because the frequency components at the Fourier plane are never completely spatially separable—although focused, every frequency component has a finite spot size which overlaps with its neighboring components—the intensity and phase modulation of the Fourier-plane mask is also not completely spectral [21]. If the modulation is sharp compared with the spot size of individual frequency components on the Fourier plane, the output beam and its focus in an experiment will suffer from a linear spatio-temporal coupling. This effect has been extensively studied in the literature, and its implications for quantum control experiments were also considered by Sussman *et al* [23]

On the other hand, if the modulation is gentle enough, the output beam will not exhibit severe spatio-temporal coupling, and so can be considered as almost purely spectrally shaped by the mask. Like a spectrometer, the 4f pulse shaper only uses one spatial dimension for dispersion, and the other orthogonal dimension is not functionally exploited. It is easy to see that, by inserting a 2D mask on the Fourier plane, one can in principle make arbitrary spatio-temporal shaping involving the additional spatial dimension. This has been demonstrated [21, 98] as a generic spatio-temporal shaper and has been applied to the coherent control of lattice responses [99] and multidimensional nonlinear spectroscopy [100]. Such spatio-temporal pulse shapers have also been successfully characterized with 2D spectral interferometry [101].

One system whose STC has been extensively studied is a focusing system containing one or many lenses [6, 25, 32]. This is of great practical interest, because most experiments require intensities only achievable by focused pulses. It is known that a focused ultrashort pulse usually suffers from radially varying pulse duration and group delay. Analytical formulae have been derived for these effects with simple lens systems.

Even without the chromatic aberration of lenses, because of the wavelength dependence of diffraction, different frequency components will usually have different spot sizes in a tightly focused beam. The spatio-temporal behavior of a polychromatic beam is a subject of theoretical interest. For example, the so-called isodiffracting beam—the natural mode of a curved mirror resonator—is found to possess the property that all frequency components have the same Rayleigh length, and its spatio-temporal evolution through the focus was studied by Feng and Winful [102]. Higher-order modes of isodiffracting pulses have also been studied [103]. The spatio-temporal behavior of subcycle pulses in a nonparaxial Gaussian beam has also been studied theoretically by Saari [104].

While theoretical results are very helpful in giving guidance to designing a good experiment, in many cases, the system or the pulse can be too complicated for an analytical calculation of the spatio-temporal effects. Numerical simulation, however, is possible for arbitrary optical systems by combining commercial ray-tracing programs with wave propagation aspects. This approach has been successfully employed to calculate the dispersion properties of arbitrary optical systems [5, 105], as well as spatio-temporal effects [35].

4.2. Exploiting STCs

In the discussions of section 4.1, we mostly described cases where STCs appear as side effects and are hence undesirable. Yet, there are also many cases which benefit from these effects.

One of the most common exploitations of STCs is the enhancement of phase matching and nonlinear optical conversion efficiencies via these couplings. In three-wave mixing experiments, the phase matching is commonly achieved by adjusting the angle between the input beams in a birefringent crystal, thereby matching the phase velocities. The group velocities, however, remain unmatched and this mismatch limits the efficiency of the process. It was shown that tilting the pulse fronts of the beams can resolve this problem and provide both phase and group velocity matched beams [106]. This is equivalent to angularly dispersing the beam so that each wavelength enters the crystal at its phase matching angle [107–110].

As an application of this method, it was shown that pulses with pulse-front tilt can significantly enhance the bandwidth of the output pulses in optical-parametric chirped-pulse amplification experiments [111]. Broadband phase matching is optimized at a certain angle between the signal and the pump beams. However, this configuration causes a strong group velocity mismatch between the two interacting pulses. Tilting of the pulse fronts of the signal in a manner to compensate for the angle with the pump provides matched group velocities over the interaction range. An analogous approach was also used to generate nearly single-cycle pulses [112].

In an analogous application, pulse-front tilt was also used to enhance the conversion efficiencies in optical-rectification experiments to generate broadband terahertz radiation [113]. Photon conversion efficiencies as high as 45% were achieved in this configuration [114].

Spatial dispersion, or the lateral separation of different frequency components in a beam, can be introduced in laser cavities to increase the bandwidth after mode locking. Spatial dispersion reduces the mode competition, favors the mode-locking process and enhances the bandwidth of the laser (and yields shorter pulse widths) [115]. Similarly, pulse-front tilt can also be used in traveling-wave excitation schemes for laser cavities [14].

'Temporal focusing' is a very interesting application of STCs that has been applied to multiphoton microscopes to reduce the amount of scanning needed to collect an image [116, 117]. In this scheme, an ultrashort laser pulse goes through a diffraction grating and a high-magnification telescope. Because negative GVD is associated with angular dispersion imposed by the grating, the pulse experiences a rapid change of pulse length and spatio-temporal couplings. Only in one particular focal plane will the pulse be temporally and spatially well focused, reaching the highest intensity; away from this focal plane, the intensity quickly drops. Therefore, the introduction and control of the spatio-temporal coupling allows much better longitudinal resolution in microscopy experiments than usual techniques. Characterization of the temporal focusing set-up has recently been performed using SEA TADPOLE [118].

Finally, another system in which STCs are generated and play a helpful role is in a filament generated by an ultrashort pulse, which is sustained by the balance between self-focusing in a nonlinear medium and the defocusing effects of ionized plasma and geometrical divergence [37]. Because self-focusing and ionization are strongly intensity-dependent, in a non-flat-top beam, radial spatio-temporal effects are obviously going to be observed in the profile of a filament. While the spatio-temporal evolution may introduce complicated temporal and spectral structure, by a careful choice of experimental parameters, these coupled effects may favor pulse self-compression and few-cycle pulses can be generated in this manner [42, 119]. It was shown that the physics behind self-compression is not the negative dispersion due to the generated plasma. Instead, it is the spatio-temporal evolution of the pulse that causes pulse splitting and favors the self-compression [120].

Recently, effects of STCs on ultrafast laser micromachining applications were also studied. It was shown that these couplings yield interesting effects such as non-reciprocal structure generation [121, 122].

5. Summary

The nearly ubiquitous nature of space–time couplings in ultrashort laser pulses and their significant contributions to light–matter interactions makes these couplings impossible to disregard. These STCs can be detrimental or beneficial. Avoiding or minimizing these effects when they are unwanted, and properly using them when they are to be exploited, requires understanding their physics and origins. In this review, we presented a summary of recent work on the description of STCs. We also elucidated several experimental methods used to measure these phenomena. Finally, we discussed practical scenarios where STCs are avoided and made use of. In short, STCs yield a very rich range of effects and provide additional, controllable parameters for many applications of ultrafast phenomena.

References

[1] Diels J C and Rudolph W 1996 *Ultrashort Laser Pulse Phenomena* (San Diego, CA: Academic)

[2] Rulliere C (ed) 1998 *Femtosecond Laser Pulses: Principles and Experiments* (Heidelberg: Springer)

[3] Zewail A 2000 Femtochemistry: atomic-scale dynamics of the chemical bond (adapted from the Nobel lecture) *J. Phys. Chem.* **39** 5660–94

[4] Gerstner E 2007 Laser physics: extreme light *Nature* **446** 16–8

[5] Druon F, Chériaux G, Faure J, Nees J, Nantel M, Maksimchuk A, Mourou G, Chanteloup J C and Vdovin G 1998 Wave-front correction of femtosecond terawatt lasers by deformable mirrors *Opt. Lett.* **23** 1043–5

[6] Bor Z 1989 Distortion of femtosecond laser pulses in lenses *Opt. Lett.* **14** 119–21

[7] Fork R L, Martinez O E and Gordon J P 1984 Negative dispersion using pair of prisms *Opt. Lett.* **9** 150–2

[8] Martinez O E, Gordon J P and Fork R L 1984 Negative group-velocity dispersion using refraction *J. Opt. Soc. Am.* B **1** 1003–6

[9] Gordon J P and Fork R L 1984 Optical resonator with negative dispersion *Opt. Lett.* **9** 153–5

[10] Treacy E 1969 Optical pulse compression with diffraction gratings *IEEE J. Quantum Electron.* **5** 454–8

[11] Martinez O E 1986 Grating and prism compressors in the case of finite beam size *J. Opt. Soc. Am.* B **3** 929–34

[12] Strickland D and Mourou G 1985 Compression of amplified chirped optical pulses *Opt. Commun.* **56** 219–21

[13] Pessot M, Maine P and Mourou G 1987 1000 times expansion/compression of optical pulses for chirped pulse amplification *Opt. Commun.* **62** 419–21

[14] Bor Z and Racz B 1985 Group velocity dispersion in prisms and its application to pulse compression and travelling-wave excitation *Opt. Commun.* **54** 165–70

[15] Martinez O E 1986 Pulse distortions in tilted pulse schemes for ultrashort pulses *Opt. Commun.* **59** 229–32

[16] Osvay K, Kovacs A P, Heiner Z, Kurdi G, Klebniczki J and Csatari M 2004 Angular dispersion and temporal change of femtosecond pulses from misaligned pulse compressors *IEEE J. Sel. Top. Quantum Electron.* **10** 213–20

[17] Akturk S, Kimmel M, O'Shea P and Trebino R 2003 Measuring pulse-front tilt in ultrashort pulses using GRENOUILLE *Opt. Express* **11** 491–501

[18] Weiner A M, Heritage J P and Kirschner E M 1988 High-resolution femtosecond pulse shaping *J. Opt. Soc. Am.* B **5** 1563–72

[19] Heritage J P, Weiner A M and Thurston R N 1985 Picosecond pulse shaping by spectral phase and amplitude manipulation *Opt. Lett.* **10** 609–11

[20] Zeek E, Maginnis K, Backus S, Russek U, Murnane M, Mourou G, Kapteyn H and Vdovin G 1999 Pulse compression by use of deformable mirrors *Opt. Lett.* **24** 493–5

[21] Wefers M M, Nelson K A and Weiner A M 1996 Multidimensional shaping of ultrafast optical waveforms *Opt. Lett.* **21** 746–8

[22] Weiner A M 2000 Femtosecond pulse shaping using spatial light modulators *Rev. Sci. Instrum.* **71** 1929

[23] Sussman B J, Lausten R and Stolow A 2008 Focusing of light following a 4f pulse shaper: considerations for quantum control *Phys. Rev.* A **77** 43416

[24] Freiberg A and Saari P 1983 Picosecond spectrochronography *IEEE J. Quantum Electron.* **19** 622–30

[25] Bor Z 1988 Distortion of femtosecond laser pulses in lenses and lens systems *J. Mod. Opt.* **35** 1907–18

[26] Bor Z and Horvath Z L 1992 Distortion of femtosecond pulses in lenses. Wave-optical description *Opt. Commun.* **94** 249–58

[27] Horvath Z L and Bor Z 1993 Focusing of femtosecond pulses having gaussian spatial distribution *Opt. Commun.* **100** 6–12

[28] Kempe M, Stamm U, Wilhelmi B and Rudolph W 1992 Spatial and temporal transformation of femtosecond laser pulses by lenses and lens systems *J. Opt. Soc. Am.* B **9** 1158–65

[29] Kempe M and Rudolph W 1993 Femtosecond pulses in the focal region of lenses *Phys. Rev.* A **48** 4721–9

[30] Federico A and Martinez O 1992 Distortion of femtosecond pulses due to chromatic aberration in lenses *Opt. Commun.* **91** 104–10

[31] Fuchs U, Zeitner U D and Tünnermann A 2006 Hybrid optics for focusing ultrashort laser pulses *Opt. Lett.* **31** 1516–8

[32] Kempe M and Rudolph W 1993 Impact of chromatic and spherical aberration on the focusing of ultrashort light pulses by lenses *Opt. Lett.* **18** 137–9

[33] Horvath Z L and Bor Z 2001 Diffraction of short pulses with boundary diffraction wave theory *Phys. Rev.* E **63** 1–11

[34] Horvath Z L, Klebniczki J, Kurdi G and Kovacs A P 2004 Experimental investigation of the boundary wave pulse *Opt. Commun.* **239** 243–50

[35] Fuchs U, Zeitner U D and Tuennermann A 2005 Ultra-short pulse propagation in complex optical systems *Opt. Express* **13** 3852–61

[36] Braun A, Korn G, Du D, Squier J and Mourou G 1995 Self-channeling of high-peak-power femtosecond laser pulses in air *Opt. Lett.* **20** 73–5

[37] Couairon A and Mysyrowicz A 2007 Femtosecond filamentation in transparent media *Phys. Rep.* **441** 47–189

[38] Zaïr A, Guandalini A, Schapper F, Holler M, Biegerti J, Gallmann L, Couairon A, Franco M, Mysyrowicz A and Keller U 1996 Spatio-temporal characterization of few-cycle pulses obtained by filamentation *Phys. Rev. Lett.* **77** 1234–7

[39] Kolesik M, Wright E M and Moloney J V 2004 Dynamic nonlinear X waves for femtosecond pulse propagation in water *Phys. Rev. Lett.* **92** 253901

[40] Mlejnek M, Wright E M and Moloney J V 1998 Dynamic spatial replenishment of femtosecond pulses propagating in air *Opt. Lett.* **23** 382–4

[41] Akturk S, Couairon A, Franco M and Mysyrowicz A 2008 Spectrogram representation of pulse self compression by filamentation *Opt. Express* **16** 17626–36

[42] Couairon A, Biegert J, Hauri C P, Kornelis W, Helbing F W, Keller U and Mysyrowicz A 2006 Self-compression of ultra-short laser pulses down to one optical cycle by filamentation *J. Mod. Opt.* **53** 75–85

[43] Mysyrowicz A, Couairon A and Keller U 2008 Self-compression of optical laser pulses by filamentation *New J. Phys.* **10** 025023

[44] Weiss C O 1992 Spatio-temporal structures. Part II. Vortices and defects in lasers *Phys. Rep.* **219** 311–38

[45] Lugiato L A 1992 Spatio-temporal structures. Part I *Phys. Rep.* **219** 293–310

[46] Hebling J 1996 Derivation of the pulse front tilt caused by angular dispersion *Opt. Quantum Electron.* **28** 1759–63

[47] Bor Z, Racz B, Szabo G, Hilbert M and Hazim H A 1993 Femtosecond pulse front tilt caused by angular dispersion *Opt. Eng.* **32** 2501–3

[48] Nabekawa Y and Midorikawa K 2002 High-order pulse front tilt caused by high-order angular dispersion *Laser* **74** S259–63

[49] Akturk S, Gu X, Zeek E and Trebino R 2004 Pulse-front tilt caused by spatial and temporal chirp *Opt. Express* **12** 4399–410

[50] Dorrer C, Kosik E M and Walmsley I A 2002 Spatio-temporal characterization of ultrashort optical pulses using two-dimensional shearing interferometry *Appl. Phys.* B **74** (suppl.) 209–19

[51] Akturk S, Gu X, Gabolde P and Trebino R 2005 The general theory of first-order spatio-temporal distortions of Gaussian pulses and beams *Opt. Express* **13** 8642–61

[52] Born M and Wolf E 1999 *Principles of Optics* 7th edn (Cambridge: Cambridge University Press)

[53] Kostenbauder A G 1990 Ray-pulse matrices: a rational treatment for dispersive optical systems *IEEE J. Quantum Electron.* **26** 1148–57

[54] Gu X, Akturk S and Trebino R 2004 Spatial chirp in ultrafast optics *Opt. Commun.* **242** 599–604

[55] Gabolde P, Lee D, Akturk S and Trebino R 2007 Describing first-order spatio-temporal distortions in ultrashort pulses using normalized parameters *Opt. Express* **15** 242–51

[56] Gradshteyn I S and Ryzhik I M 1994 *Table of Integrals, Series and Products* (New York: Academic)

[57] Varjú K, Kovács A P, Kurdi G and Osvay K 2002 High-precision measurement of angular dispersion in a CPA laser *Appl. Phys.* B **74** 259–63

[58] Trebino R 2002 *Frequency-Resolved Optical Gating: The Measurement of Ultrashort Laser Pulses* (Boston, MA: Kluwer Academic)

[59] Akturk S, Kimmel M, O'Shea P and Trebino R 2003 Measuring spatial chirp in ultrashort pulses using single-shot frequency-resolved optical gating *Opt. Express* **11** 68–78

[60] Pretzler G, Kasper A and Witte K J 2000 Angular chirp and tilted light pulses in CPA lasers *Appl. Phys.* B **70** 1–9

[61] Simon P, Gerhardt H and Szatmari S 1991 Interferometric method for the characterization of the phase and pulse fronts of femtosecond pulses *Opt. Quantum Electron.* **23** 73–9

[62] Sacks Z, Mourou G and Danielius R 2001 Adjusting pulse-front tilt and pulse duration by use of a single-shot autocorrelator *Opt. Lett.* **26** 462–4

[63] Raghuramaiah M, Sharma A K, Naik P A and Gupta P D 2003 Simultaneous measurement of pulse-front tilt and pulse duration of a femtosecond laser beam *Opt. Commun.* **223** 163–8

[64] Sharma A K, Patidar R K, Raghuramaiah M, Naik P A and Gupta P D 2006 Measuring pulse-front tilt in ultrashort pulse laser beams without ambiguity of its sign using single-shot tilted pulse-front autocorrelator *Opt. Express* **14** 13131–41

[65] O'Shea P, Kimmel M, Gu X and Trebino R 2001 Highly simplified device for ultrashort-pulse measurement *Opt. Lett.* **26** 932–4

[66] Kubota T, Komai K, Yamagiwa M and Awatsuiji Y 2007 Moving picture recording and observation of three-dimensional image of femtosecond light pulse propagation *Opt. Express* **15** 14348–54

[67] Andreoni A, Bondani M and Potenza M A C 1998 Ultra-broadband and chirp-free frequency doubling in beta-barium borate *Opt. Commun.* **154** 376–82

[68] Froehly C, Lacourt A and Vienot J C 1973 Time impulse response and time frequency response of optical pupils *Nouv. Rev. Opt.* **4** 183–96

[69] Lepetit L, Cheriaux G and Joffre M 1995 Linear techniques of phase measurement by femtosecond spectral interferometry for applications in spectroscopy *J. Opt. Soc. Am.* B **12** 2467–74

[70] Fittinghoff D N, Bowie J L, Sweetser J N, Jennings R T, Krumbügel M A, DeLong K W, Trebino R and

Walmsley I A 1996 Measurement of the intensity and phase of ultraweak, ultrashort laser pulse *Opt. Lett.* **21** 884–6
[71] Birge J R, Ell R and Kärtner F X 2006 Two-dimensional spectral shearing interferometry for few-cycle pulse characterization *Opt. Lett.* **31** 2063–5
[72] Diddams S A, Eaton H K, Zozulya A A and Clement T S 1998 Full-field characterization of femtosecond pulses after nonlinear propagation *Conf. on Lasers and Electro-Optics OSA Technical Digest*
[73] Jasapara J and Rudolph W 1999 Characterization of sub-10-fs pulse focusing with high-numerical-aperture microscope objectives *Opt. Lett.* **24** 777–9
[74] Amir W, Planchon T A, Durfee C G, Squier J A, Gabolde P, Trebino R and Mueller M 2006 Simultaneous visualizations of spatial and chromatic abberations by two-dimensional Fourier transform spectral interferometry *Opt. Lett.* **31** 2927–9
[75] Amir W, Durfee C G, Schafer D N, Gibson E A, Kost L, Przekwas E, Jimenez R and Squier J A 2008 Linear spatio-temporal characterization of a UV microscope objective for nonlinear imaging and spectroscopy by using two-dimensional spectral interferometry *J. Microsc.* **230** 4–8
[76] Adams D E, Planchon T A, Hrin A, Squier J A and Durfee C G 2009 Characterization of coupled nonlinear spatiospectral phase following an ultrafast self-focusing interaction *Opt. Lett.* **34** 1294–6
[77] Planchon T A, Childress C, Squier J A and Durfee C G 2008 Measurement of pump-induced transient lensing in a cryogenically-cooled high average power Ti: sapphire amplifier *Opt. Express* **16** 18557–64
[78] Gallmann L, Steinmeyer G, Sutter D H, Rupp T, Iaconis C, Walmsley I A and Keller U 2001 Spatially resolved amplitude and phase characterization of femtosecond optical pulses *Opt. Lett.* **26** 96–8
[79] Dorrer C, Kosik E M and Walmsley I A 2002 Direct space–time characterization of the electric fields of ultrashort optical pulses *Opt. Lett.* **27** 548–50
[80] Dorrer C, Joffre M, Jean-Pierre L and Belabas N 2000 Spectral resolution and sampling issues in Fourier-transform spectral interferometry *J. Opt. Soc. Am.* B **17** 1790–802
[81] Geindre J P, Audebert P, Rebibo S and Gauthier J C 2001 Single-shot spectral interferometry with chirped pulses *Opt. Lett.* **26** 1612–4
[82] Meshulach D, Yelin D and Silbergerg Y 1997 Real-time spatial-spectral interference measurements of ultrashort optical pulses *J. Opt. Soc. Am.* B **14** 2095–8
[83] Bowlan P, Gabolde P, Shreenath A, McGresham K, Trebino R and Akturk S 2006 Crossed-beam spectral interferometry: a simple, high-spectral-resolution method for completely characterizing complex ultrashort pulses in real time *Opt. Express* **14** 11892–900
[84] Kosik E M, Radunsky A S, Wamsley I and Dorrer C 2005 Interferometric technique for measuring broadband ultrashort pulses at the sampling limit *Opt. Lett.* **30** 326–8
[85] Bowlan P, Gabolde P, Coughlan M A, Trebino R and Levis R J 2008 Measuring the spatiotemporal electric field of ultrashort pulses with high spatial and spectral resolution *J. Opt. Soc. Am.* B **25** A81–92
[86] Bowlan P, Valtna-Lukner H, Lõhmus M, Piksarv P, Saari P and Trebino R 2009 Measuring the spatiotemporal field of ultrashort Bessel-X pulses *Opt. Lett.* **34** 2276–8
[87] Bowlan P, Fuchs U, Trebino R and Zeitner U D 2008 Measuring the spatiotemporal electric field of tightly focused ultrashort pulses with sub-micron spatial resolution *Opt. Express* **16** 13663–75
[88] Schnars U and Juptner W P O 2002 Digital recording and numerical reconstruction of holograms *Meas. Sci. Technol.* **13** 85–101
[89] Gabolde P and Trebino R 2004 Self-referenced measurement of the complete electric field of ultrashort pulses *Opt. Express* **12** 4423–9
[90] Gabolde P and Trebino R 2006 Single-shot measurement of the full spatio-temporal field of ultrashort pulses with multi-spectral digital holography *Opt. Express* **14** 11460–7
[91] Bragheri F, Faccio D, Bonaretti F, Lotti A, Clerici M, Jedrkiewicz O, Liberale C, Henin S, Tartara L and Degiorgio V 2008 Complete retrieval of the field of ultrashort optical pulses using the angle–frequency spectrum *Opt. Lett.* **33** 2952–4
[92] Grunwald R, Kebbel V, Griebner U, Neumann U, Kummrow A, Rini M, Nibbering E T J, Piché M, Rousseau G and Fortin M 2003 Generation and characterization of spatially and temporally localized few-cycle optical wavepackets *Phys. Rev.* A **67** 51
[93] Bonaretti F, Faccio D, Clerici M, Biegert J and Di Trapani P 2009 Spatiotemporal amplitude and phase retrieval of Bessel-X pulses using a Hartmann–Shack sensor *Opt. Express* **17** 9804–9
[94] Rubino E, Faccio D, Tartara L, Bates P K, Chalus O, Clerici M, Bonaretti F, Biegert J and Di Trapani P 2009 Spatiotemporal amplitude and phase retrieval of space–time coupled ultrashort pulses using the Shackled-FROG technique *Opt. Lett.* **34** 3854–6
[95] Balistreri M L M, Gersen H, Korterik J P, Kuipers L and Hulst N F V 2001 Tracking femtosecond laser pulses in space and time *Science* **294** 550–3
[96] Engelen R J P, Sugimoto Y, Gersen H, Ikeda N, Asakawa K and Kuipers L K 2007 Ultrafast evolution of photonic eigenstates in *k*-space *Nat. Phys.* **3** 401–5
[97] Akturk S, Gu X, Kimmel M and Trebino R 2006 Extremely simple single-prism ultrashort-pulse compressor *Opt. Express* **14** 10101–8
[98] Feurer T, Vaughan J C, Koehl R M and Nelson K A 2002 Multidimensional control of femtosecond pulses by use of a programmable liquid-crystal matrix *Opt. Lett.* **27** 652–4
[99] Feurer T, Vaughan J C and Nelson K A 2003 Spatiotemporal coherent control of lattice vibrational waves *Science* **299** 374
[100] Hornung T, Vaughan J C, Feurer T and Nelson K A 2004 Degenerate four-wave mixing spectroscopy based on two-dimensional femtosecond pulse shaping *Opt. Lett.* **29** 2052–4
[101] Amir W, Planchon T A, Durfee C G and Squier J A 2007 Complete characterization of a spatiotemporal pulse shaper with two-dimensional Fourier transform spectral interferometry *Opt. Lett.* **32** 939–41
[102] Feng S and Winful H G 2000 Spatiotemporal structure of isodiffracting ultrashort electromagnetic pulses *Phys. Rev.* E **61** 862–73
[103] Feng S and Winful H G 2001 Higher-order transverse modes of ultrashort isodiffracting pulses *Phys. Rev.* E **63** 46602
[104] Saari P 2001 Evolution of subcycle pulses in nonparaxial Gaussian beams *Opt. Express* **8** 590–8
[105] O'Shea D C 2006 Group velocity dispersion using commercial optical design programs *Appl. Opt.* **45** 4740–6
[106] Smith A V 2001 Group-velocity-matched three-wave mixing in birefringent crystals *Opt. Lett.* **26** 719–21
[107] Martinez O E 1989 Achromatic phase matching for second harmonic generation offemtosecond pulses *IEEE J. Quantum Electron.* **25** 2464–8
[108] Richman B A, Bisson S E, Trebino R, Mitchell M G, Sidick E and Jacobson A 1997 Achromatic phase matching for tunable second-harmonic generation by use of a prism *Opt. Lett.* **22** 1223–5
[109] Richman B A, Bisson S E, Trebino R, Sidick E and Jacobson A 1998 Efficient broadband second-harmonic generation by dispersive achromatic nonlinear conversion using prisms *Opt. Lett.* **23** 497–9
[110] Szabo G and Bor Z 1990 Broadband frequency doubler for femtosecond pulses *Appl. Phys.* B **50** 51–4

[111] Arisholm G, Biegert J, Schlup P, Hauri C P and Keller U 1989 Ultra-broadband chirped-pulse optical parametric amplifier with angularly dispersed beams *IEEE J. Quantum Electron.* **25** 2464–8
[112] Shirakawa A, Sakane I, Takasaka M and Kobayashi T 1999 Visible sub-5-fs pulse generation by pulse-front-matched optical parametric amplification *Conf. on Lasers and Electro-Optics* (Optical Society of America) Talk CTuF5
[113] Kozma I, Almasi G and Hebling J 2003 Geometrical optical modeling of femtosecond setups having angular dispersion *Appl. Phys.* B **76** 257–61
[114] Yeh K L, Hoffmann M C, Hebling J and Nelson K A 2007 Generation of 10 J ultrashort terahertz pulses by optical rectification *Appl. Phys. Lett.* **90** 171121
[115] Christov I P, Stoev V, Murnane M M and Kapteyn H C 1995 Mode-locking with a compensated space–time astigmatism *Opt. Lett.* **20** 2111–3
[116] Oron D, Tal E and Silberberg Y 2005 Scanningless depth-resolved microscopy *Opt. Express* **13** 1468–76
[117] Oron D and Silberberg Y 2005 Spatiotemporal coherent control using shaped, temporally focused pulses *Opt. Express* **13** 9903–8
[118] Coughlan M A, Plewicki M and Levis R J 2009 Parametric spatio-temporal control of focusing laser pulses *Opt. Express* **17** 15808–20
[119] Couairon A, Franco M, Mysyrowicz A, Biegert J and Keller U 2006 Pulse self-compression to the single-cycle limit by filamentation in a gas with a pressure gradient *Opt. Lett.* **30** 2657–9
[120] Akturk S, Zhou B, Pasquiou B, Franco M and Mysyrowicz A 2008 Intensity distribution around the focal regions of real axicons *Opt. Commun.* **281** 4240–4
[121] Kazansky P G, Yang W, Bricchi E, Bovatsek J, Arai A, Shimotsuma Y, Miura K and Hirao K 2007 'Quill' writing with ultrashort light pulses in transparent materials *Appl. Phys. Lett.* **90** 151120
[122] Yang W, Kazansky P G and Svirko Y P 2008 Non-reciprocal ultrafast laser writing *Nature Photon.* **2** 99–104